Dark energy model with very large-scale inhomogeneity

Yue Nan[1] and Kazuhiro Yamamoto[2,3]

[1]*Department of Physics, Graduate School of Science, Hiroshima University, Higashi-Hiroshima 739-8526, Japan*

[2]*Department of Physics, Kyushu University, 744 Motooka, Nishi-Ku, Fukuoka 819-0395, Japan*

[3]*Research Center for Advanced Particle Physics, Kyushu University, 744 Motooka, Nishi-ku, Fukuoka 819-0395, Japan*

(Received 26 April 2021; accepted 22 February 2022; published 16 March 2022)

We consider a dynamical model for dark energy based on an ultralight mass scalar field with very large-scale inhomogeneities. This model may cause observable impacts on the anisotropic properties of the cosmic microwave background (CMB) intensity and luminosity distance. We formulate the model as the cosmological perturbations of the superhorizon scales, focusing on the local region of our universe. Moreover, we investigated the characteristic properties of the late-time evolution of inhomogeneous dark energy. Our numerical solutions show that the model can mimic the standard ΛCDM cosmology while including spatially dependent dark energy with flexible ranges of the model parameters. We put a constraint on the amplitude of these inhomogeneities of the dark energy on very large scales with the observations of the CMB anisotropies. We also discuss their influence on the estimation of the luminosity distance.

DOI: 10.1103/PhysRevD.105.063518

I. INTRODUCTION

The observations of the redshifts of the distant Type Ia supernovae (SNe Ia) imply the existence of an unknown repulsive interaction that accelerates the expansion of the universe in relatively late times [1–5]; otherwise, this fact suggests the breakdown of general relativity on cosmological scales. To account for these observations, dark energy has become an essential component of cosmology since the late 1990s, in addition to the cold dark matter (CDM) [6]. Albert Einstein first introduced a cosmological constant Λ into general relativity to establish a static universe. Since the expansion of the universe was discovered and the big-bang cosmology became a paradigm after the discovery of the cosmic microwave background (CMB), the cosmological constant Λ was revived and discussed occasionally (see Ref. [7] for a review). The cosmological constant Λ is now included in the standard model of cosmology as the simplest model of dark energy to explain the accelerated expansion, which has also been tested by observing the CMB and baryon acoustic oscillations (BAO) in the context of structure formation theories [8]. The scenario is summarized as the well-known standard ΛCDM cosmological model [9,10], where dark energy consists of approximately 70% of the total energy density of the universe at the present epoch.

Many dark energy models have been proposed as variants of the cosmological constant, where the equation of state (EoS) ω is defined by the ratio of pressure p to energy density ρ as $\omega = p/\rho$ is a typical quantity used to characterize the property of the dark energy. Early observations of SNe Ia constrained that $\omega < -1/3$ for dark energy, which have been followed by more precise observations, suggesting that the dark energy EoS would be very close to the cosmological constant, with $\omega = -1$. As the energy density of radiation ρ_r and matter ρ_m decays with $\rho_r \propto a^{-4}$, $\rho_m \propto a^{-3}$ with the scale factor of the universe a, and dark energy seems to behave as an almost constant and homogeneous background of the universe, its energy density is suggested to become dominant in the late times of the universe when $a \gtrsim 0.5$. Hence, the property of dark energy is important for the evolution of the universe, especially in the late times and in the future.

The large-scale structure of matter distributions serves as a useful probe for dark energy EoS because the BAO signature is useful as a standard ruler. Furthermore, the growth of clustering of the matter is affected by dark energy. On the other hand, these also gave rise to another mysterious aspect of dark energy as a famous fine-tuning problem, i.e., "cosmological constant problem" (see Refs. [6,7]). The problem is why the dark energy density is of the same order as the matter density at the present epoch, much smaller than the prediction from a naive expectation of modern particle physics theories, while its EoS implies linkage with the vacuum energy of quantum fields. These problems may be closely related to the origin and nature of dark energy, which remains to be explored.

Many theoretical models of dark energy have been investigated [6,8], in which dynamical models are very interesting [11–18], because they are related to the field theory associated with the primordial high-energy epoch of

the universe and fundamental theories of theoretical physics [6,7,19]. Particularly interesting ones are the dynamical models based on the quantum fluctuations of ultralight scalar fields [12–18], which reveal an interesting connection to the string axiverse scenario [20–27]. As in the ΛCDM model and in many models of dark energy, a basic assumption of their property is spatial isotropy and homogeneity, which follows the cosmological principle. Nevertheless, since the late-time expansion of the universe is dominated by dark energy, some interesting outcomes may occur to affect cosmological observables if large-scale inhomogeneities of dark energy arise, which could be tested by various cosmological observations [19,28–31].

On the other hand, anomalous features in the CMB anisotropies have been pointed out by some authors [32,33]. Although the cosmic variance limits the ability for our precise comparison between theoretical predictions and observations, there is the possibility that the low CMB multipoles provide us with a clue for physics beyond the standard cosmological model for dark energy [34,35]. The general interpretation for the CMB dipole anisotropy is our peculiar motion toward a CMB rest frame, related to a dragging toward the great attractor in the sky; at least part of the peculiar motions is interpreted as evidence of gravitational bounding [36,37]. The latest result shows the validity of the interpretation of the CMB dipole by the peculiar motion [38]. However, the result does not necessarily mean that all of the CMB dipole anisotropy could be entirely explained by the canonical scenario of peculiar motion [39,40]. We will present a dark energy model with very large-scale inhomogeneities, including an intrinsic dipole component as a possible solution.

Recently, the Hubble tension problem has also garnered attention due to the precision of the observations. The present expansion rate H_0 locally measured from standard candles, such as SNe Ia [41] and that inferred from the BAO statistics on CMB fluctuations [10,42], has shown nontrivial deviations from each other. Many attempts have been made to ease or explain this tension, and among them still stands out the possibility that this tension is related to new physics concerning dark energy beyond the standard ΛCDM model [43]. Recent investigations using scaling relations of galaxy clusters in Refs. [44,45] reported that the variation in luminosity distance d_L appears to exist in different regions of the sky, potentially suggesting anisotropy in the local expansion rate H_0, whose line was followed by Refs. [46,47]. Some correlation of H_0 anomalies with the CMB dipole direction is commonly implied by these works, which also facilitates the motivation of our work.

To shed light on the problems concerning dark energy, the authors investigated a model for dark energy with large-scale stochastic fluctuations assumed in an open universe associated with a specific inflationary scenario [48]. These fluctuations will be translated into large-scale spatial inhomogeneities and time-dependent dark energy EoS in the evolution of the universe. In the present work, we consider a general dynamical model for dark energy with large-scale spatial inhomogeneities consisting of a scalar field ϕ by handling them in the framework of the cosmological perturbation theory. This model may introduce some observable effects on the anisotropies of the cosmological observations to address the problems concerning the dark energy property mentioned previously.

The remainder of this paper is organized as follows. In Sec. II, we propose a basic formulation for the model and its cosmological setups. Then, we use the formulation to derive the Einstein equations for the system as well as the equations of motion: for both the dark energy represented by the dynamical scalar field ϕ and the matter component in the late-time universe. In Sec. III, we use the analytic approximations to solve for the equations in the limit $a \ll 1$, where a denotes the scale factor of the universe. This is useful to determine the necessary initial conditions for the numerical solution to the late-time cosmological evolution of the system. In Sec. IV, we consider the possible effects of large-scale dark energy fluctuations on cosmological observations, such as the CMB temperature power spectra and luminosity distance. Section V is devoted to summarizing our results and brief discussions. The appendixes provide additional explanations for specific technical details. In Appendix A, explicit forms of the matrices used in the definition of the perturbations are presented, and their relations with multipole expansion are discussed. In Appendix B, we show the consistency of the derived equations with previous works [48,49], especially for the superhorizon Euler equation of the matter component. Appendix C provides additional details for the background solutions and the analytic approximations. Appendix D shows the dark energy EoS in our model and its relation to the Chevallier-Polarski-Linder (CPL) parametrization [50,51]. In Appendix E, we show that our application of the model to the correction of the luminosity distance is valid and consistent with previous works [52,53]. Finally, in Appendix F, we present a helpful toolkit for transforming equations between forms with respect to different variables in our model.

II. BASIC FORMULATION

In the present paper, motivated by a previous model with supercurvature-mode dark energy associated with an open universe scenario [17,18,54], we consider the evolution of dark energy with superhorizon large-scale inhomogeneities and its possible imprints on cosmological observations by characterizing the inhomogeneities analytically. To formulate these inhomogeneities, we start with following the cosmological setup of metric perturbations.

A. Fundamental setups

The characteristic feature of the dark energy model previously proposed in Refs. [48,54] is the spatial inhomogeneities of the dark energy density on the very large scales. Following the scenario, such large-scale spatial inhomogeneities of dark energy originated from the vacuum fluctuations of the supercurvature modes of a scalar field during an open inflationary scenario [54,55]. An ultralight scalar field ϕ with spatial fluctuations taking a nonlinear amplitude on the supercurvature scales is responsible for the dark energy in the scenario. Because the horizon size of our universe is much smaller than the scales of the inhomogeneities of the dark energy, the breaking of the cosmological principle is small within the observable universe, which might enable us to escape from the observational constraints.

In the present paper, we formulate a phenomenological model of dark energy that slightly breaks the cosmological principle by mimicking the previous model [48,54]. We consider a dark energy model of a scalar field spatially varying on the superhorizon scales on the spatially flat background universe, for simplicity, by assuming

$$ds^2 = a^2(\eta)[-(1+2\Psi)d\eta^2 + (1+2\Phi)\delta_{ij}dx^i dx^j], \tag{1}$$

where δ_{ij} is the Kronecker delta δ_{ij}, $a(\eta)$ is the scale factor of the universe with the conformal time η, and Ψ and Φ are the metric perturbations that we want to characterize later.

Now, we set the cosmological metric perturbation as Ψ, considering only the large-scale superhorizon mode perturbations. In Ref. [48], it was discussed that the inhomogeneities induced by superhorizon fluctuations are dominated by dipole and quadrupole components among all possible contributions. Now, neglecting higher multipoles, we can explicitly write out the metric perturbations as

$$\Psi = \epsilon_1 \sum_{m=1}^{3} \Psi_{1(m)}(\eta) P_i^{(m)} x^i + \epsilon_2 \sum_{m=1}^{5} \Psi_{2(m)}(\eta) P_{ij}^{(m)} x^i x^j, \tag{2}$$

$$\Phi = \epsilon_1 \sum_{m=1}^{3} \Phi_{1(m)}(\eta) P_i^{(m)} x^i + \epsilon_2 \sum_{m=1}^{5} \Phi_{2(m)}(\eta) P_{ij}^{(m)} x^i x^j, \tag{3}$$

$$\phi = \phi_0(\eta) + \epsilon_1 \sum_{m=1}^{3} \phi_{1(m)}(\eta) P_i^{(m)} x^i + \epsilon_2 \sum_{m=1}^{5} \phi_{2(m)}(\eta) P_{ij}^{(m)} x^i x^j, \tag{4}$$

where $P_i^{(m)}$ and $P_{ij}^{(m)}$ are the vectors of traceless matrices related to the multipole expansion of the perturbations to the spatial basis, whose expressions are explicitly given in Appendix A. We use ϕ to denote the ultralight scalar field we assume as the source of dark energy with large-scale spatial inhomogeneities. Here ϵ_1 and ϵ_2 are introduced to explicitly express the order of perturbations for the dipole and the quadrupole, which can be included in the perturbations. We set ϵ_1 and ϵ_2 to be unity later. Considering a standard CDM scenario, we can write the perturbations for the matter density distribution as

$$\rho = \rho_0(\eta) + \epsilon_1 \sum_{m=1}^{3} \rho_{1(m)}(\eta) P_i^{(m)} x^i + \epsilon_2 \sum_{m=1}^{5} \rho_{2(m)}(\eta) P_{ij}^{(m)} x^i x^j, \tag{5}$$

and we define the velocity field as

$$u_i \equiv \partial_i \bar{V}, \tag{6}$$

with constraints $u_\mu u^\mu = -1$, where $\bar{V}$ is the velocity potential, which is expressed as

$$\bar{V} = \epsilon_1 \sum_{m=1}^{3} V_{1(m)}(\eta) P_i^{(m)} x^i + \epsilon_2 \sum_{m=1}^{5} V_{2(m)}(\eta) P_{ij}^{(m)} x^i x^j. \tag{7}$$

Here $\Psi_{\ell(m)}, \Phi_{\ell(m)}, \phi_{\ell(m)}, \rho_{\ell(m)}, V_{\ell(m)}$ with $\ell = 1, 2$ are the coefficients of the dipole and the quadrupole components, and ϕ_0 and ρ_0 are the background quantities.

B. Essence of the equations

The evolution of the system is described by the Einstein equations

$$G^\mu{}_\nu = 8\pi G(T^{(\phi)\mu}{}_\nu + T^{(\mathrm{M})\mu}{}_\nu), \tag{8}$$

with the energy momentum tensors for the scalar field with mass m and the matter component

$$T^{(\phi)}_{\mu\nu} = \partial_\mu\phi\partial_\nu\phi - g_{\mu\nu}\left(\frac{1}{2}g^{\alpha\beta}\partial_\alpha\phi\partial_\beta\phi + \frac{1}{2}m_\phi^2\phi^2\right),$$
$$T^{(\mathrm{M})}_{\mu\nu} = \rho u_\mu u_\nu, \tag{9}$$

and the equations of motion for the scalar field ϕ and the conservation law for the matter component

$$\frac{1}{\sqrt{-g}}\partial_\mu(\sqrt{-g}g^{\mu\nu}\partial_\nu\phi) - m_\phi^2\phi = 0, \tag{10}$$

$$\nabla_\mu T^{(\mathrm{M})\mu}{}_\nu = 0. \tag{11}$$

The EoS of the dark energy field ϕ is an important quantity characterizing its properties and evolution. From the standard formula for the energy density and the pressure of a scalar field, taking the form of a scalar field potential

$V(\phi) = m_\phi^2\phi^2/2$ into account we obtain the equation of state ω_ϕ as

$$\omega_\phi \equiv \frac{P_\phi}{\rho_\phi} \simeq -\frac{2a^2V(\phi) - \dot{\phi}^2}{2a^2V(\phi) + \dot{\phi}^2} = -\frac{m_\phi^2a^2\phi^2 - \dot{\phi}^2}{m_\phi^2a^2\phi^2 + \dot{\phi}^2}, \quad (12)$$

where the dot denotes the differentiation with respect to the conformal time η. Here we neglected the contribution from the spatial variations, which is small in our case. The EoS depends on the dynamical evolution of ϕ and is a concordant generalization to the CPL parametrization (see Appendix D) [50,51].

The linear expansion of Eqs. (2)–(4) ensures that Eqs. (8)–(11) give the same form as equations for each multipole component with indices $\ell = 1, 2$ and $m = 1, 2, 3, 4, 5$. Indeed, the components with different ℓ indices, for example, $\Psi_{\ell=1}$ and $\Psi_{\ell=2}$, have different dimensions to the order of length by definition. Keeping this fact in mind, for simplicity of the notations, we neglect indices (m) in the following parts and use only the lower indices ℓ to denote the multipole components of these perturbations. In the following parts, we use lower indices 0 for the background quantities and ℓ for the perturbations on the superhorizon scales.

Using the conformal Hubble parameter $\mathcal{H} = aH(a) = \dot{a}/a$ instead of Hubble parameter $H(a)$, Eq. (10) yields

$$\ddot{\phi}_0 + 2\mathcal{H}\dot{\phi}_0 + m_\phi^2a^2\phi_0 = 0, \quad (13)$$

$$\ddot{\phi}_\ell + 2\mathcal{H}\dot{\phi}_\ell + m_\phi^2a^2\phi_\ell + \dot{\phi}_0(3\dot{\Phi}_\ell - \dot{\Psi}_\ell - 4\mathcal{H}\Psi_\ell) - 2\ddot{\phi}_0\Psi_\ell = 0. \quad (14)$$

On the other hand, Eq. (11) leads to

$$3\mathcal{H}\rho_0 + \dot{\rho}_0 = 0, \quad (15)$$

$$3\mathcal{H}\rho_\ell + \dot{\rho}_\ell + 3\rho_0\dot{\Phi}_\ell = 0, \quad (16)$$

$$\dot{V}_\ell - a\Psi_\ell = 0. \quad (17)$$

By defining the density perturbation as $\rho_\ell \equiv \rho_0\delta_\ell$, it is obvious that Eqs. (15) and (16) are consistent with those obtained from the continuity equation, and Eq. (25) in Ref. [48] at a large-scale limit. It is worth mentioning that the velocity equation in Eq. (17) is also consistent with Eq. (26) in Ref. [48], which is obtained from the Euler equation (see Appendix B).

Defining $M_{\rm pl}^{-2} \equiv 8\pi G$ for short, the Einstein equations can be written as

$$-3\mathcal{H}^2 + M_{\rm pl}^{-2}\left(\frac{1}{2}m_\phi^2a^2\phi_0^2 + \frac{1}{2}\dot{\phi}_0^2 + a^2\rho_0\right) = 0, \quad (18)$$

$$\mathcal{H}^2 - 2\frac{\ddot{a}}{a} + M_{\rm pl}^{-2}\left(\frac{1}{2}m_\phi^2a^2\phi_0^2 - \frac{1}{2}\dot{\phi}_0^2\right) = 0, \quad (19)$$

$$-2(\mathcal{H}\Psi_\ell - \dot{\Phi}_\ell) + M_{\rm pl}^{-2}(a\rho_0V_\ell + \dot{\phi}_0\phi_\ell) = 0, \quad (20)$$

$$6\mathcal{H}(\mathcal{H}\Psi_\ell - \dot{\Phi}_\ell) + M_{\rm pl}^{-2}(a^2\rho_\ell + m_\phi^2a^2\phi_0\phi_\ell - \dot{\phi}_0(\dot{\phi}_0\Psi_\ell - \dot{\phi}_\ell)) = 0, \quad (21)$$

$$\left(2\frac{\ddot{a}}{a} - \mathcal{H}^2\right)\Psi_\ell + \mathcal{H}\dot{\Psi}_\ell - 2\mathcal{H}\dot{\Phi}_\ell - \dot{\Phi}_\ell + \frac{M_{\rm pl}^{-2}}{2}(m_\phi^2a^2\phi_0\phi_\ell + \dot{\phi}_0(\dot{\phi}_0\Psi_\ell - \dot{\phi}_\ell)) = 0. \quad (22)$$

We can classify these equations by the order of the perturbations, dividing them into the background equations that read

$$\dot{\rho}_0 + 3\mathcal{H}\rho_0 = 0, \quad (23)$$

$$\ddot{\phi}_0 + 2\mathcal{H}\dot{\phi}_0 + m_\phi^2a^2\phi_0 = 0, \quad (24)$$

$$-3\mathcal{H}^2 + M_{\rm pl}^{-2}\left(\frac{1}{2}m_\phi^2a^2\phi_0^2 + \frac{1}{2}\dot{\phi}_0^2 + a^2\rho_0\right) = 0, \quad (25)$$

$$\mathcal{H}^2 - 2\frac{\ddot{a}}{a} + M_{\rm pl}^{-2}\left(\frac{1}{2}m_\phi^2a^2\phi_0^2 - \frac{1}{2}\dot{\phi}_0^2\right) = 0, \quad (26)$$

and first-order perturbative equations relying on the background as follows:

$$\dot{\rho}_\ell + 3\mathcal{H}\rho_\ell + 3\rho_0\dot{\Phi}_\ell = 0, \quad (27)$$

$$\ddot{\phi}_\ell + 2\mathcal{H}\dot{\phi}_\ell + m_\phi^2a^2\phi_\ell + \dot{\phi}_0(3\dot{\Phi}_\ell - \dot{\Psi}_\ell - 4\mathcal{H}\Psi_\ell) - 2\ddot{\phi}_0\Psi_\ell = 0, \quad (28)$$

$$\dot{V}_\ell - a\Psi_\ell = 0, \quad (29)$$

$$-2(\mathcal{H}\Psi_\ell - \dot{\Phi}_\ell) + M_{\rm pl}^{-2}(a\rho_0V_\ell + \dot{\phi}_0\phi_\ell) = 0, \quad (30)$$

$$6\mathcal{H}(\mathcal{H}\Psi_\ell - \dot{\Phi}_\ell) + M_{\rm pl}^{-2}(a^2\rho_\ell + m_\phi^2a^2\phi_0\phi_\ell - \dot{\phi}_0(\dot{\phi}_0\Psi_\ell - \dot{\phi}_\ell)) = 0, \quad (31)$$

$$\left(2\frac{\ddot{a}}{a} - \mathcal{H}^2\right)\Psi_\ell + \mathcal{H}\dot{\Psi}_\ell - 2\mathcal{H}\dot{\Phi}_\ell - \ddot{\Phi}_\ell + \frac{M_{\rm pl}^{-2}}{2}(m_\phi^2a^2\phi_0\phi_\ell + \dot{\phi}_0(\dot{\phi}_0\Psi_\ell - \dot{\phi}_\ell)) = 0. \quad (32)$$

After solving for the background, we can find out the evolution of large-scale perturbations originated from the fluctuations of the dark energy field ϕ.

III. ANALYTIC APPROXIMATIONS AND NUMERICAL SOLUTIONS

In this section, we consider solving the evolution equations obtained in the previous section for both the background and the perturbations. Because we are interested in the late-time evolution after the last scattering ($a_d \sim 1/1100$), we first find the analytic approximates of the solutions based in the matter-dominant epoch, which are useful as the initial conditions for numerical evaluation when $a_d \lesssim a \ll 1$.

A. The background evolution

First, we must solve the background evolution of our system in Eqs. (23)–(26) before considering the perturbations, which should yield cosmological observational constraints that models close to the ΛCDM models are favored. Moreover, we must use the observed value of the Hubble parameter at the present epoch to determine the dark energy density of the field ϕ.

Using these approximates we may infer the initial conditions of the background for numerical solutions of the background evolution.

To parametrize the equations, we introduce the cosmic time t by $dt = ad\eta$. Defining tilde dimensionless quantities as

$$\tilde{t} \equiv H_0 t, \tag{33}$$

$$\tilde{\phi}_0 \equiv \phi_0/\bar{\phi}_0, \tag{34}$$

$$\tilde{r} \equiv \frac{1}{6}(\bar{\phi}_0/M_{\rm pl})^2, \tag{35}$$

$$\tilde{m} \equiv m_\phi/H_0, \tag{36}$$

$$\tilde{H} \equiv H/H_0, \tag{37}$$

we can obtain dimensionless ordinary differential equations using $\tilde{t}$ as an independent variable as

$$\tilde{r}\tilde{m}^2\tilde{\phi}_0^2(\tilde{t}) + \tilde{r}\left(\frac{\mathrm{d}\tilde{\phi}_0}{\mathrm{d}\tilde{t}}\right)^2 + \Omega_m a^{-3} = \left(\frac{1}{a}\frac{\mathrm{d}a}{\mathrm{d}\tilde{t}}\right)^2, \tag{38}$$

$$\frac{\mathrm{d}^2\tilde{\phi}_0}{\mathrm{d}\tilde{t}^2} + 3\frac{1}{a}\frac{\mathrm{d}a}{\mathrm{d}\tilde{t}}\frac{\mathrm{d}\tilde{\phi}_0}{\mathrm{d}\tilde{t}} + \tilde{m}^2\tilde{\phi}_0 = 0, \tag{39}$$

where H_0 is the Hubble constant and $\bar{\phi}_0$ is a constant related to the initial value of ϕ_0. If we use the scale factor a instead of t, and use superscript $'$ to denote the derivative with respect to scale factor a, then the equations correspond to

$$(1 - \tilde{r}a^2\tilde{\phi}_0'^2)\tilde{H}^2 = \tilde{r}\tilde{m}^2\tilde{\phi}_0^2 + \Omega_m a^{-3}, \tag{40}$$

$$a^2\tilde{H}^2\tilde{\phi}_0'' + (4a\tilde{H}^2 + a^2\tilde{H}\tilde{H}')\tilde{\phi}_0' + \tilde{m}^2\tilde{\phi}_0 = 0. \tag{41}$$

Following Eq. (40) we may also write out the dimensionless expansion rate as

$$\tilde{H}(a) = \sqrt{\frac{\tilde{r}\tilde{m}^2\tilde{\phi}_0^2 + \Omega_m a^{-3}}{1 - \tilde{r}a^2\tilde{\phi}_0'^2}}. \tag{42}$$

We leave more details of procedures of solving these background equations to Appendix C. It is worth noting that according to the definitions in Eqs. (33)–(36), there are 2 degrees of freedom for the parameters $\tilde{m}$ and $\tilde{r}$, to specify the mass and energy scale of the dark energy field ϕ, respectively. The unknown component in our model, dark energy ϕ, can be fundamentally characterized by two parameters. One is the shape of its potential $V(\phi) = m_\phi^2\phi^2/2$, and the other is the initial value in our universe, while the properties of the other component (e.g., matter) are considered as known under the standard cosmological model.

In order to fix the dark energy density today, we have the constraint from the present Hubble rate by definitions

$$a(\tilde{t}_0) = a(H_0 t_0) \equiv 1, \tag{43}$$

$$H(\tilde{t}_0) = H(H_0 t_0) \equiv H_0, \tag{44}$$

where t_0 is the proper cosmic time for the present epoch. Inserting this into Eq. (38) actually gives

$$1 - \Omega_m = \tilde{r}\tilde{m}^2(\tilde{\phi}_0|_{\tilde{t}=\tilde{t}_0})^2 + \tilde{r}\left(\frac{\mathrm{d}\tilde{\phi}_0}{\mathrm{d}\tilde{t}}\bigg|_{\tilde{t}=\tilde{t}_0}\right)^2. \tag{45}$$

Equation (45) is the necessary condition for specifying the dark energy density observed today when solving the background equations. Together with Eqs. (38) and (39), the system is now prepared for numerical evaluation to obtain the evolution of $a(\tilde{t})$ and $\tilde{\phi}_0(\tilde{t})$. As we are mainly interested in the late-time evolution here, we can determine the initial value for independent variables $\tilde{t}$ or a (to be discussed later) manually as a typical value; for example, $a_i = a_d \approx 1/1100$ at the photon decoupling off the last scattering, by use of Eq. (C2). These solutions determine the background evolution that we rely on to solve the perturbation equations.

It is worth mentioning that Eq. (45) also provides a particular baseline for choosing the parameters $\tilde{m}$ and $\tilde{r}$ from the various parameter spaces, and that the case for the choice of parameters approximating the ΛCDM model is

$$\tilde{r}\tilde{m}^2 \simeq 1 - \Omega_m, \tag{46}$$

concerning which more details can be found in Appendix C [see also Eq. (48)]. However, this condition for parameter choice is not mandatory to solve for the system.

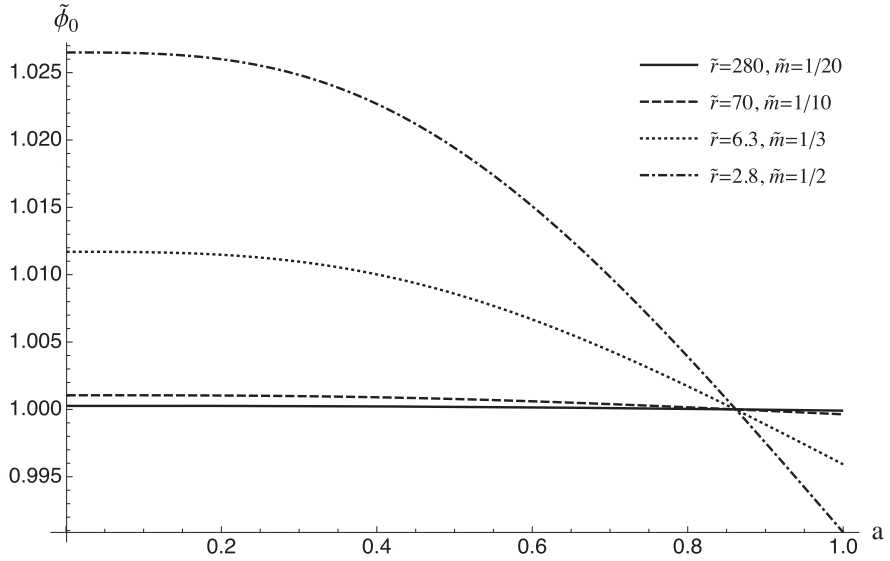

FIG. 1. An example of the evolution of the background solutions $\tilde{\phi}_0(a)$ as a function of the scale factor a with the different sets of parameters for $\tilde{r}$ and $\tilde{m}$ presented in the figure, which mimic ΛCDM universes with $\Omega_m = 0.3$ using Eq. (46). Notice that each model has different initial values for $\tilde{\phi}_0$. We observe from the figure that the lighter field ϕ is more "frozen" in its evolutionary history because $\tilde{m}$ is normalized by the Hubble constant in Eq. (36). Here, the curve with $\tilde{m} = 1/20$ and $\tilde{r} = 280$ is most similar to the cosmological constant model among the curves.

We can now solve for $\tilde{\phi}_0(a)$ numerically under 2 degrees of freedom for the choice of parameters $\tilde{m}$ and $\tilde{r}$. Examples of the solutions under the conditions that allow the recovery of the models close to the ΛCDM universe are presented in Figs. 1 and 2. To investigate the impact of parameter choices on the background solutions more specifically, we also chose other sets of parameters. Table I provides the parameter sets adopted in the present paper. The cosmological parameter Ω_m is related to the fixing of dark energy density at the present epoch, hence slightly affecting $\tilde{\phi}_0$ if it is not fixed, which is shown in Fig. 3. We present some typical figures showing how parameters can affect the equation of state ω_ϕ as a function of a in Figs. 4 and 5, where $\tilde{r}$ is not important (see discussions on ω_ϕ later). Figures 6 and 7 demonstrate the background expansion rate predicted under different parameters.

We now discuss the behaviors of the background solutions under different parameters. Figure 1 shows the

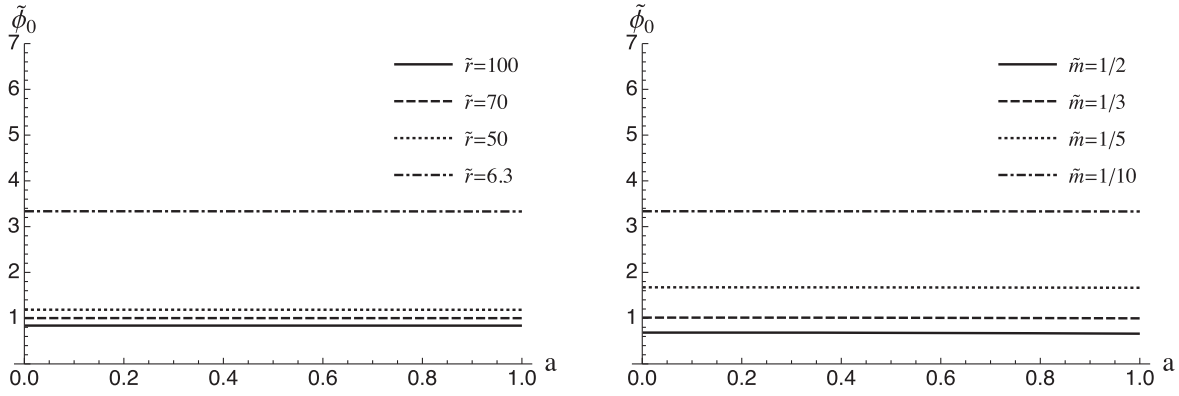

FIG. 2. Although the parameters in Fig. 1 seem to be the most natural choices for $\tilde{m}$ and $\tilde{r}$, there could be other possibilities. The left panel of this figure shows the impact of the value of $\tilde{r}$ on the evolution of the background solution $\tilde{\phi}_0(a)$ as a function of a with fixed $\tilde{m} = 1/10$. According to Eq. (35), $\tilde{r}$ reflects the value of the scalar field ϕ. Hence, this panel demonstrates that the background solution is almost constant, whereas its value, taking $\phi_0 \gtrsim M_{\rm pl}$, depends on $\tilde{r}$. In contrast, the right panel shows the impact of the value of $\tilde{m}$ on the evolution of the background solution $\tilde{\phi}_0(a)$ as a function of a, where we fixed $\tilde{r} = 6.3$. Recalling Eq. (36), $\tilde{m}$ is the parameter of the field mass. These behaviors can be comprehended by Eqs. (47) and (50), where $\tilde{r}$ and $\tilde{m}$ act similarly to some rescaling factors of $\tilde{\phi}_0$. The two parameters correspond to the 2 degrees of freedom for the potential shape of ϕ, whose parameter space is constrained by the observed dark energy density [see Eq. (45)] and determines the late-time dynamics of ϕ until the present epoch, which is assumed to be mild.

TABLE I. Numerical results with different model parameters $(\tilde{r}, \tilde{m})$ and cosmological parameter Ω_m. The models close to the ΛCDM model are labeled as Nos. (1), (2), (7), (8), (9), (10), (13), and (14). Within these models, Nos. (1), (2), (7), (8), (9), and (10) satisfy the condition in Eq. (46) with exact holding of the equality. Note that the values for the present comoving horizon η_0 also indicate that $\tilde{r}$ is not important for the background expansion, while Ω_m does show its expected influence on η_0. To see this, we focus on comparing the conditions of the models labeled with Nos. (1), (3), (4), (6), and (11), where different values of $\tilde{r}$ rarely change η_0; on the other hand, a comparison among Nos. (1), (13), and (14) shows a slight dependence of η_0 on Ω_m, as expected. Especially, No. (11) is a model extremely close to the ΛCDM model, and the EoS of dark energy is almost constant $w_\phi \approx -1$, predicting a future evolution quickly approaching the de Sitter expansion.

No.	$(\tilde{r}, \tilde{m})$	Ω_m	$Q_{1(m)}$	$Q_{2(m)}$	$\varepsilon_1^{\max}$	$\varepsilon_2^{\max}$	$F_{S1(m)}(z=3)$	$F_{S2(m)}(z=3)$	$H_0\eta_0$
(1)	$(70, 1/10)$	0.30	−0.107	−0.0895	1.17×10^{-2}	5.72×10^{-5}	−0.0462	−0.0693	3.19
(2)	$(6.3, 1/3)$	0.30	−0.107	−0.0896	1.17×10^{-2}	5.71×10^{-5}	−0.0462	−0.0692	3.19
(3)	$(50, 1/10)$	0.30	−0.0904	−0.0757	1.39×10^{-2}	6.76×10^{-5}	−0.0390	−0.0586	3.19
(4)	$(100, 1/10)$	0.30	−0.128	−0.107	9.82×10^{-3}	4.78×10^{-5}	−0.0552	−0.0828	3.19
(5)	$(6.3, 1/5)$	0.30	−0.0642	−0.0537	1.96×10^{-2}	9.52×10^{-5}	−0.0277	−0.0416	3.19
(6)	$(6.3, 1/10)$	0.30	−0.0321	−0.0269	3.91×10^{-2}	1.91×10^{-4}	−0.0138	−0.0208	3.19
(7)	$(2.8, 1/2)$	0.30	−0.107	−0.0897	1.18×10^{-2}	5.70×10^{-5}	−0.0463	−0.0692	3.19
(8)	$(280, 1/20)$	0.30	−0.107	−0.0895	1.17×10^{-2}	5.72×10^{-5}	−0.0461	−0.0693	3.19
(9)	$(72, 1/10)$	0.28	−0.116	−0.100	1.08×10^{-2}	5.11×10^{-5}	−0.0503	−0.0770	3.28
(10)	$(68, 1/10)$	0.32	−0.0985	−0.0803	1.27×10^{-2}	6.37×10^{-5}	−0.0425	−0.0626	3.11
(11)	$(1/70, 1/10)$	0.30	−0.00153	−0.00128	8.21×10^{-1}	4.00×10^{-5}	−0.000659	−0.000990	3.19
(12)	$(6.3, 1/2)$	0.30	−0.160	−0.135	7.83×10^{-3}	3.80×10^{-5}	−0.0694	−0.104	3.19
(13)	$(70, 1/10)$	0.32	−0.100	−0.0815	1.25×10^{-2}	6.28×10^{-5}	−0.0431	−0.0635	3.11
(14)	$(70, 1/10)$	0.28	−0.115	−0.0988	1.09×10^{-2}	5.18×10^{-5}	−0.0496	−0.07594	3.28

impact of the parameter choice on the behavior of the solution for $\tilde{\phi}_0(a)$ in the cases following Eq. (46), where models close to the ΛCDM cosmologies are expected. Figure 2 shows how the parameters $\tilde{r}$ and $\tilde{m}$ affect the behaviors of $\tilde{\phi}_0$, while Fig. 3 shows how Ω_m can affect $\tilde{\phi}_0$. The behaviors of the $\tilde{\phi}_0$ curves in these figures can be understood as follows. From Eqs. (38) and (45) we can see that the parameter $\tilde{r}$ can actually be absorbed into the amplitude of $\tilde{\phi}_0$ as a rescaling factor, namely

$$\tilde{m}^2(\sqrt{\tilde{r}}\tilde{\phi}_0)^2 + \left(\frac{\mathrm{d}(\sqrt{\tilde{r}}\tilde{\phi}_0)}{\mathrm{d}\tilde{t}}\right)^2 = \left(\frac{1}{a}\frac{\mathrm{d}a}{\mathrm{d}\tilde{t}}\right)^2 - \Omega_m a^{-3}, \quad (47)$$

with

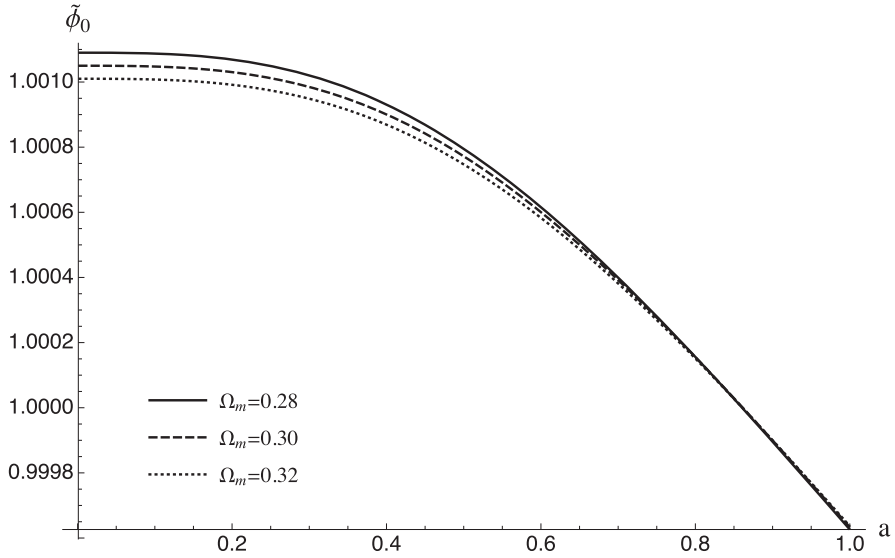

FIG. 3. Impact of Ω_m on the evolution of the background solution $\tilde{\phi}_0(a)$. Here, we fixed $\tilde{r} = 70$ and $\tilde{m} = 1/10$. As expected, Ω_m only alter the evolution to a slight extent, suggesting that our model solutions are robust against changes in Ω_m.

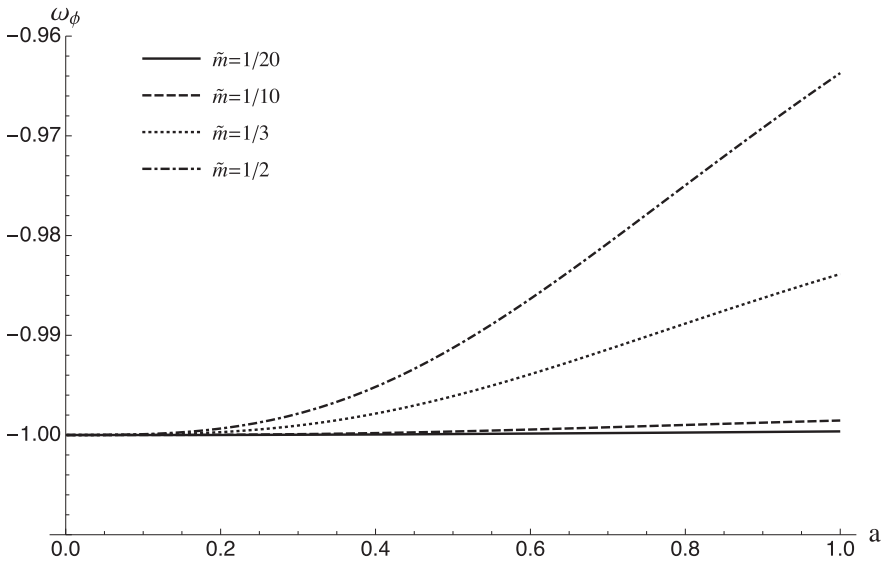

FIG. 4. Evolution of the dark energy EoS $\omega_\phi(a)$ with the different sets of the parameters chosen in Fig. 1. From Eqs. (45) and (D3), it is straightforward to see that $\tilde{r}$ does not affect the EoS of $\tilde{\phi}_0$. The figure shows the influence of $\tilde{m}$ on the EoS of $\tilde{\phi}_0$ with fixed $\Omega_m = 0.3$.

$$1 - \Omega_m = \tilde{m}^2(\sqrt{\tilde{r}}\tilde{\phi}_0|_{a=1})^2 + (\sqrt{\tilde{r}}\tilde{\phi}_0{}'|_{a=1})^2. \quad (48)$$

These two equations facilitate understanding why changing $\tilde{r}$ with other parameters fixed only alters the value of $\tilde{\phi}_0$ without causing a nontrivial difference in the characteristic behaviors of the curves in Fig. 2. Moreover, as we evaluate $\tilde{\phi}_0$, choosing the condition in Eq. (46) close to the ΛCDM model as a baseline for the natural choices of the parameters,

$$\frac{\mathrm{d}(\sqrt{\tilde{r}}\tilde{\phi}_0)}{\mathrm{d}\tilde{t}} \ll 1 \quad \text{or} \quad \sqrt{\tilde{r}}\tilde{\phi}_0{}' \ll 1 \quad (49)$$

always holds. Hence, it follows Eq. (47) that

$$(\sqrt{\tilde{r}}\tilde{m}\tilde{\phi}_0)^2 \simeq \left(\frac{1}{a}\frac{\mathrm{d}a}{\mathrm{d}\tilde{t}}\right)^2 - \Omega_m a^{-3}. \quad (50)$$

Because of similar arguments for $\tilde{r}$, we understand that, to some extent, $\tilde{m}$ also works as a rescaling factor for the background $\tilde{\phi}_0$, which explains the behavior of $\tilde{\phi}_0$ in Fig. 2. At the same time, the appearance of Ω_m on the right-hand side of Eq. (50) explains the dependence of the background solution $\tilde{\phi}_0$ on Ω_m in Fig. 3.

Now, let us discuss the parameter dependence of the dark energy EoS $\omega_\phi(a)$, as shown in Figs. 4 and 5. We may conclude that the background dark energy EoS $\omega_\phi(a)$ is almost independent of $\tilde{r}$; in contrast, $\tilde{m}$ is the main influencing factor. There is also a slight dependence on

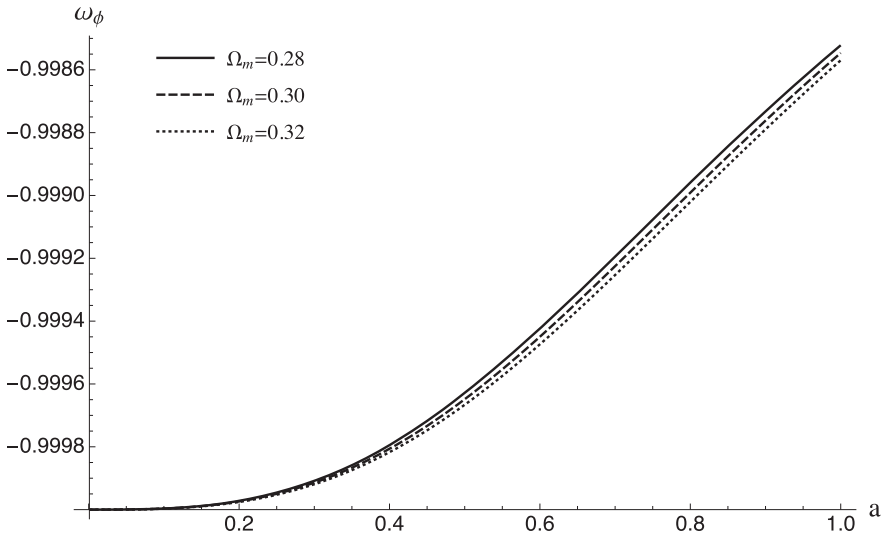

FIG. 5. This figure demonstrates the weak dependence of the EoS on Ω_m with $\tilde{m} = 1/10$ and $\tilde{r} = 70$ fixed.

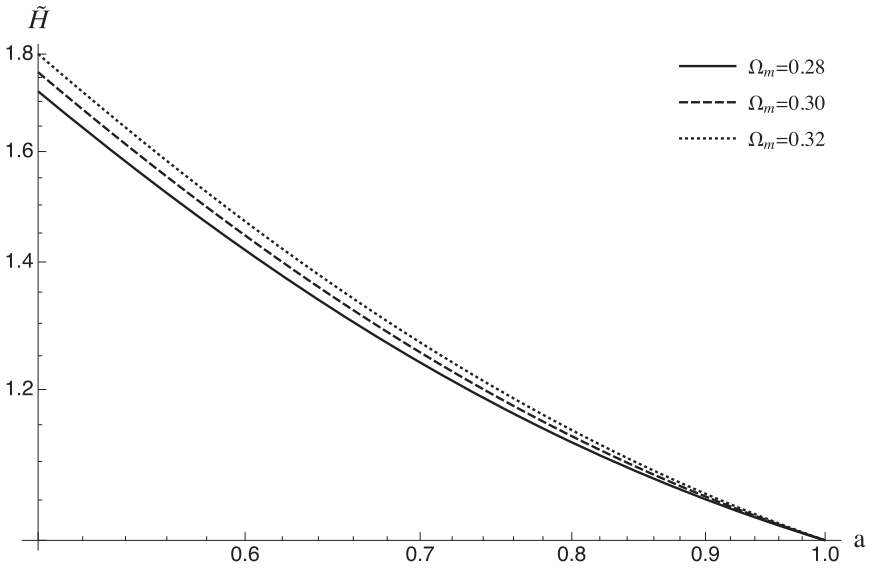

FIG. 6. Examples of the late-time expansion history $\tilde{H}(a)$ as a function of a for $0.5 \leq a \leq 1$ with different sets of Ω_m, $\tilde{r} \approx 70$ but with $\tilde{m} = 1/10$ fixed. For the late-time expansion history, only Ω_m is important.

the cosmological parameter Ω_m, as shown in Fig. 5. These behaviors can be understood using Eqs. (D1)–(D4) in Appendix D as an analogy to the CPL parametrization. Generally, $\omega_\phi(a) \simeq -1 + 2(1 - (a\tilde{m}^2\tilde{\phi}_0^2)/(\Omega_m\tilde{\phi}_0{}'^2))$ holds for almost all models; hence, $\tilde{r}$ does not have an impact on ω_ϕ at the background level, while $\tilde{m}$ and Ω_m do affect the dark energy EoS ω_ϕ.

Figure 6 shows a slight dependence on Ω_m for the expansion rate $\tilde{H}(a)$ as a function of the scale factor for $0.5 < a < 1$, while Fig. 7 shows a possible impact on the future expansion rate from the mass parameter $\tilde{m}$. To explain these behaviors for $\tilde{H}(a)$, let us consider the analytic approximation of $\tilde{H}(a)$ starting from Eq. (42). For models close to the ΛCDM model, where $\tilde{\phi}_0 \simeq$ const and $\tilde{\phi}_0{}' \simeq 0$ with Eq. (46), reading $\tilde{r}\tilde{m}^2 \simeq 1 - \Omega_m$ holds, we have

$$\tilde{H}(a) \simeq \sqrt{(1 - \Omega_m)\tilde{\phi}_0^2 + \Omega_m a^{-3}}, \tag{51}$$

which is almost the same as the Hubble equation for the standard ΛCDM parametrization. Hence, it is obvious that Ω_m is the dominant parameter for the background expansion history when $0 < a < 1$.

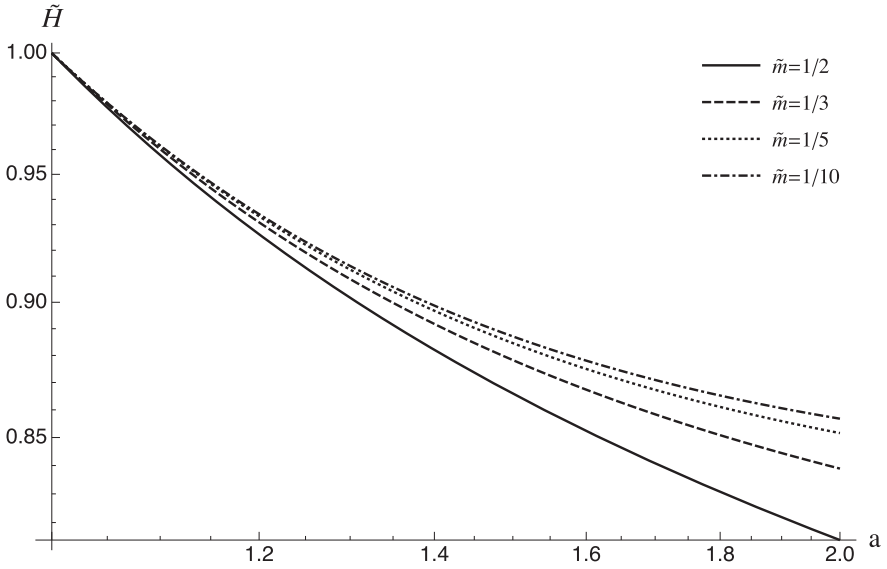

FIG. 7. Future evolution of the expansion rate. The parameter $\tilde{m}$ is only important for future expansion when $1 \ll a$. The figure demonstrates examples of how the future expansion rate depends on $\tilde{m}$ for $1 < a < 2$, where $\tilde{r} = 6.3$ and $\Omega_m = 0.3$ are fixed.

B. Equations governing first-order perturbations

In the previous subsection, we have solved for the background, and on the basis of the background solutions we now consider the numerical solution for the first-order perturbation equations in Eqs. (27)–(32) that we are interested in.

We define the perturbation to dark matter density as

$$\rho_\ell \equiv \rho_0 \delta_\ell, \tag{52}$$

together with the following quantity associated with the velocity as

$$\tilde{V}_\ell \equiv H_0 V_\ell. \tag{53}$$

Then, we can utilize the Friedmann equation relation in Eqs. (27)–(32) to eliminate quantities such as ρ_0 and ρ_ℓ, and use δ_ℓ to characterize the first-order matter perturbations as

$$\rho_0(a) = 3H_0^2 \Omega_m a^{-3} M_{\rm pl}^2. \tag{54}$$

Thus the dimensionless differential equations as functions of $\tilde{t}$ will be

$$\frac{\partial \delta_\ell}{\partial \tilde{t}} + 3\frac{\partial \Phi_\ell}{\partial \tilde{t}} = 0, \tag{55}$$

$$\frac{\partial^2 \tilde{\phi}_\ell}{\partial \tilde{t}^2} + \frac{3}{a}\frac{\partial a}{\partial \tilde{t}}\frac{\partial \tilde{\phi}_\ell}{\partial \tilde{t}} + \tilde{m}^2 \tilde{\phi}_\ell - 2\Psi_\ell \frac{\partial^2 \tilde{\phi}_0}{\partial \tilde{t}^2} - \frac{6\Psi_\ell}{a}\frac{\partial a}{\partial \tilde{t}}\frac{\partial \tilde{\phi}_0}{\partial \tilde{t}} + \frac{\partial}{\partial \tilde{t}}(3\Phi_\ell - \Psi_\ell)\frac{\partial \tilde{\phi}_0}{\partial \tilde{t}} = 0, \tag{56}$$

$$\frac{\partial \tilde{V}_\ell}{\partial \tilde{t}} - \Psi_\ell = 0, \tag{57}$$

$$-\frac{2}{a}\frac{\partial a}{\partial \tilde{t}}\Psi_\ell + 2\frac{\partial \Phi_\ell}{\partial \tilde{t}} + 3\tilde{V}_\ell \Omega_m a^{-3} + 6\tilde{r}\tilde{\phi}_\ell \frac{\partial \tilde{\phi}_0}{\partial \tilde{t}} = 0, \tag{58}$$

$$6\left(\frac{1}{a}\frac{\partial a}{\partial \tilde{t}}\right)^2 \Psi_\ell - 6\left(\frac{1}{a}\frac{\partial a}{\partial \tilde{t}}\right)\frac{\partial \Psi_\ell}{\partial \tilde{t}} + 3\Omega_m a^{-3}\delta_\ell + 6\tilde{r}\left(\tilde{m}^2 \tilde{\phi}_0 \tilde{\phi}_\ell + \frac{\partial \tilde{\phi}_0}{\partial \tilde{t}}\frac{\partial \tilde{\phi}_\ell}{\partial \tilde{t}} - \Psi_\ell\left(\frac{\partial \tilde{\phi}_0}{\partial \tilde{t}}\right)^2\right) = 0, \tag{59}$$

$$\left(\left(\frac{1}{a}\frac{\partial a}{\partial \tilde{t}}\right)^2 + \frac{2}{a}\frac{\partial^2 a}{\partial \tilde{t}^2}\right)\Psi_\ell + \frac{1}{a}\frac{\partial a}{\partial \tilde{t}}\frac{\partial}{\partial \tilde{t}}(\Psi_\ell - 3\Phi_\ell) - \frac{\partial^2 \Phi_\ell}{\partial \tilde{t}^2} + 3\tilde{r}\left(\tilde{m}^2 \tilde{\phi}_0 \tilde{\phi}_\ell - \frac{\partial \tilde{\phi}_0}{\partial \tilde{t}}\frac{\partial \tilde{\phi}_\ell}{\partial \tilde{t}} + \Psi_\ell\left(\frac{\partial \tilde{\phi}_0}{\partial \tilde{t}}\right)^2\right) = 0. \tag{60}$$

Notice that from Eq. (55)

$$\delta_\ell + 3\Phi_\ell = \text{const}, \tag{61}$$

where the constant is presumed to be zero as we assume that the superhorizon perturbations of the scalar field are the isocurvature perturbations. Then, we assume the initial values

$$\delta_\ell(0) = \Phi_\ell(0) = 0. \tag{62}$$

As in the case of the supercurvature mode dark energy [48], if we adopt the general condition that anisotropic stress is negligible, which reads

$$\Phi_\ell + \Psi_\ell \simeq 0, \tag{63}$$

we can eliminate Φ_ℓ and Ψ_ℓ using δ_ℓ and $\partial \tilde{V}_\ell / \partial \tilde{t}$ using Eq. (57). Finally, we will have two equations for δ_ℓ and $\tilde{\phi}_\ell$ to solve, whose explicit forms are long and trivial; hence, we omit them here. We note that our analysis is based on the conformal Newtonian (longitudinal) gauge, which is widely used in various analyses of cosmological perturbations. It is known that the conformal Newtonian gauge leaves no residual gauge freedom except for the long wavelength mode of $k = 0$. The effect of the inhomogeneities of our dark energy model is the isocurvature perturbations in the long wavelength limit. We consider that the gauge freedom is fixed for the dipole and quadrupole modes with nonzero small k; however, the possibility of contamination by the gauge modes with $k = 0$ could be mentioned.

Again, we need to consider the initial conditions for which we solve the equations in the limit $a \ll 1$ in an analytic manner. First, recalling the definition of Eqs. (4) and (34), we can generalize the dimensionless quantities as

$$\phi \equiv \overline{\phi}_0 \left(\tilde{\phi}_0 + \epsilon_1 \tilde{\phi}_1 \sum_m P_i^{(m)} x^i + \epsilon_2 \tilde{\phi}_2 \sum_m P_{ij}^{(m)} x^i x^j\right). \tag{64}$$

In the limit $a \ll 1$ ($t \to 0, \tilde{t} \to 0$), we may assume the power law form for the perturbations

$$\delta_\ell \equiv A_1 \tilde{t}^\alpha, \tag{65}$$

$$\tilde{\phi}_\ell \equiv \mathcal{D} + D_1 \tilde{t}^\gamma. \tag{66}$$

Furthermore, Eq. (C5) gives

$$\tilde{\phi}_0(\tilde{t}) = C_1 \frac{\sin(\tilde{m}\,\tilde{t})}{\tilde{m}\,\tilde{t}} \approx C_1\left(1 - \frac{\tilde{m}^2 \tilde{t}^2}{6}\right) \equiv F\left(1 - \frac{\tilde{m}^2 \tilde{t}^2}{6}\right). \tag{67}$$

For a given $\tilde{m}$ and $\tilde{r}$, we solve for the background and fix the value for C_1 or F in Sec. III A. We may take F as a known quantity here. For scale factor a, recall that Eq. (C2) is the background analytical approximation as

$$a = \left(\frac{9}{4}\Omega_m\right)^{\frac{1}{3}}\tilde{t}^{\frac{2}{3}} \equiv B\tilde{t}^{\frac{2}{3}}, \qquad \tilde{t} = \left(\frac{a}{B}\right)^{\frac{3}{2}}.$$

Inserting the ansatz Eqs. (65)–(67) into Eqs. (56)–(60) will give us equations as a function of a or $\tilde{t}$ relating the unknown coefficients α, γ, A_1, $\mathcal{D}$, D_1 that we want to explore. For the limit $a \to 0$ or $\tilde{t} \to 0$, by looking at the leading order of a for each equation, we have

$$\alpha = \gamma = 2, \tag{68}$$

$$D_1 = -\frac{1}{6}\tilde{m}^2\mathcal{D}, \tag{69}$$

$$A_1 = -\frac{27}{22}\tilde{m}^2\tilde{r}F\mathcal{D}, \tag{70}$$

where $\mathcal{D}$ may be understood as the amplitude of each mode of the perturbations as ϵ_1 and ϵ_2, which will be constrained later with the observational data. For now, $\mathcal{D} = 1$ may be set for the numerical solution.

Further, the analytic approximations for the evolution of the perturbations in the limit $a \ll 1$ ($t \to 0, \tilde{t} \to 0$) are found as

$$\delta_\ell \simeq -\frac{27}{22}\mathcal{D}\tilde{m}^2\tilde{r}F\tilde{t}^2 = -\frac{27}{22}\tilde{m}^2\tilde{r}F\tilde{t}^2, \tag{71}$$

$$\tilde{\phi}_\ell \simeq \mathcal{D}\left(1 - \frac{1}{6}\tilde{m}^2\tilde{t}^2\right) = 1 - \frac{1}{6}\tilde{m}^2\tilde{t}^2, \tag{72}$$

allowing us to set the proper initial conditions for δ_ℓ and $\tilde{\phi}_\ell$. The equations using a and $\tilde{t}$ as independent variables are mutually transformable using Eq. (C2), as was done in Sec. III A. The analytical solution of the first-order equations in Eqs. (27)–(32) for the other quantities can be found in a similar way as

$$\Phi_\ell \simeq -\Psi_\ell \simeq +\frac{9}{22}\mathcal{D}\tilde{m}^2\tilde{r}F\tilde{t}^2 = +\frac{9}{22}\tilde{m}^2\tilde{r}F\tilde{t}^2, \tag{73}$$

$$\tilde{V}_\ell \simeq -\frac{3}{22}\mathcal{D}\tilde{m}^2\tilde{r}F\tilde{t}^3 = -\frac{3}{22}\tilde{m}^2\tilde{r}F\tilde{t}^3. \tag{74}$$

We notice that δ_ℓ and Ψ_ℓ are negative values, which correspond to the positive values of $\tilde{\phi}_\ell$ in Eq. (72). Physically, this means that an increase in dark energy ϕ makes the matter density perturbations δ_ℓ (curvature potentials Φ_ℓ) negative (positive).

The first-order equations (27)–(32) can be solved in an exact manner using a numerical method. We present examples of the numerical solutions for perturbations $\tilde{\phi}_\ell(a)$ and $\delta_\ell(a)$ in Fig. 8, where we adopted $\mathcal{D} = 1$ with the same typical parameter sets $\tilde{r}$ and $\tilde{m}$ chosen in Sec. III A. The consistency between the analytic approximations in Eqs. (71) and (72) (dashed line) with the numerical results (solid line) when $a \lesssim 0.5$ corresponding to the matter-dominant initial condition is also demonstrated in Fig. 8, while the analytic approximation deviates from the numerical solution when $a \gtrsim 0.5$.

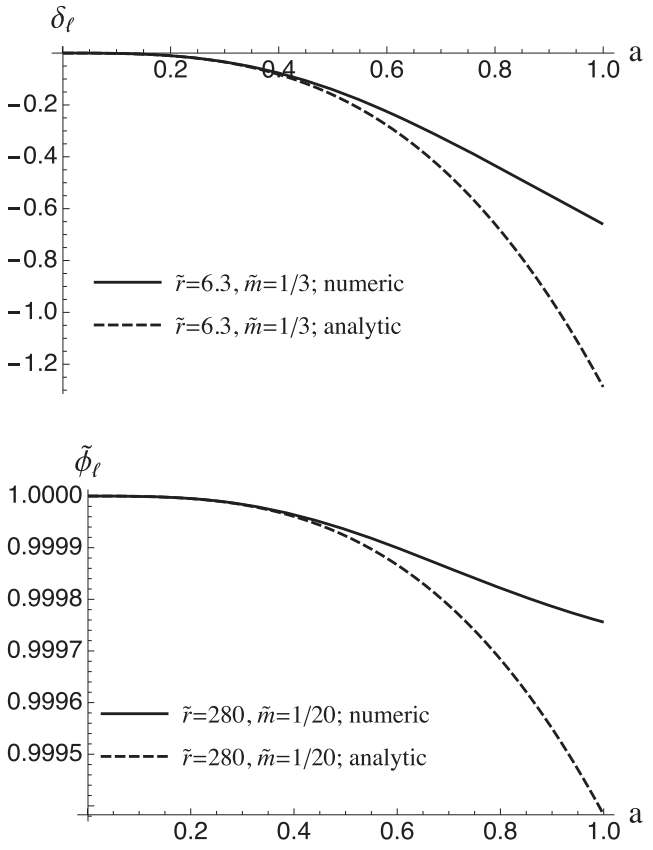

FIG. 8. Comparison of the evolution of δ_ℓ and $\tilde{\phi}_\ell$ between the analytic approximation (dashed curve) by Eqs. (71) and (72), and the exact numerical solutions (solid curves). Here, we adopt $\tilde{r} = 70$ and $\tilde{m} = 1/10$ for δ_ℓ, and $\tilde{r} = 280$ and $\tilde{m} = 1/20$ for $\tilde{\phi}_\ell$ as examples. We checked the validity of the analytic approximations for other values of $\tilde{m}$ and $\tilde{r}$ adopted in Table I. The deviation between the analytic approximation and the numerical solution starting around $a \gtrsim 0.5$ arises from the emerging domination of dark energy, which breaks down the analytic approximation obtained from the initial condition of matter domination.

We show how $\tilde{m}$ affects the solution $\tilde{\phi}_\ell$ in Fig. 9. It should be noted that there is a slight dependence on Ω_m for $\tilde{\phi}_\ell$, similar to the behavior of $\tilde{\phi}_0$ in Fig. 3. The behaviors of $\tilde{\phi}_\ell$ can be roughly understood from Eq. (72), which is valid for $a \lesssim 0.5$. Here $\tilde{m}$ is important for the evolution of $\tilde{\phi}_\ell$, whereas $\tilde{r}$ is not. On the other hand, Eq. (28) indicates that the solution of $\tilde{\phi}_\ell$ depends on $\tilde{\phi}_0$; hence, it slightly depends on Ω_m, which can be understood by a discussion similar to that on the behavior of $\tilde{\phi}_0$ in Sec. III A [see Eq. (50)].

The dependence on the parameters for δ_ℓ is shown in Fig. 10. From Eq. (71), we can conclude that $\tilde{m}$ and $\tilde{r}$ affect

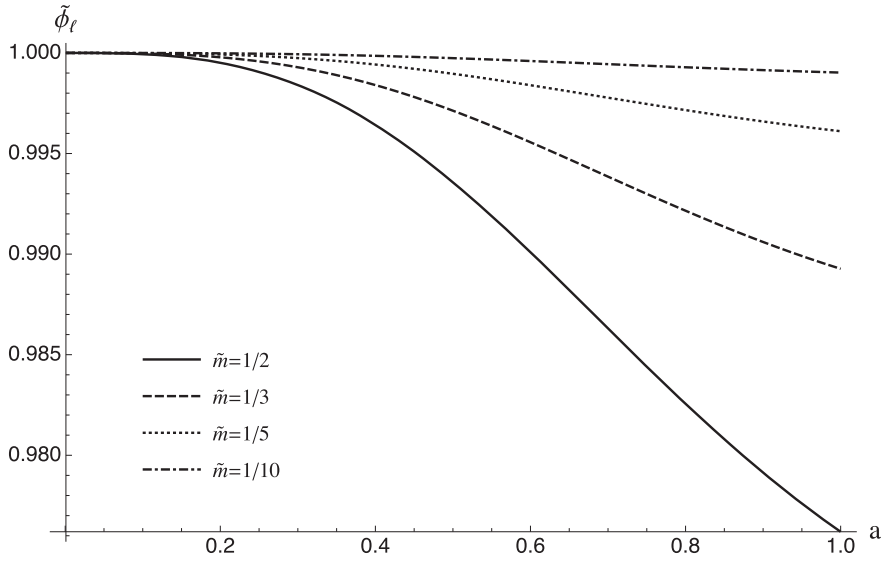

FIG. 9. Numerical solutions for the perturbation for $\tilde{\phi}_\ell(a)$, with the different values of parameter $\tilde{m}$, where $\Omega_m = 0.3$ and $\tilde{r} = 6.3$ are fixed.

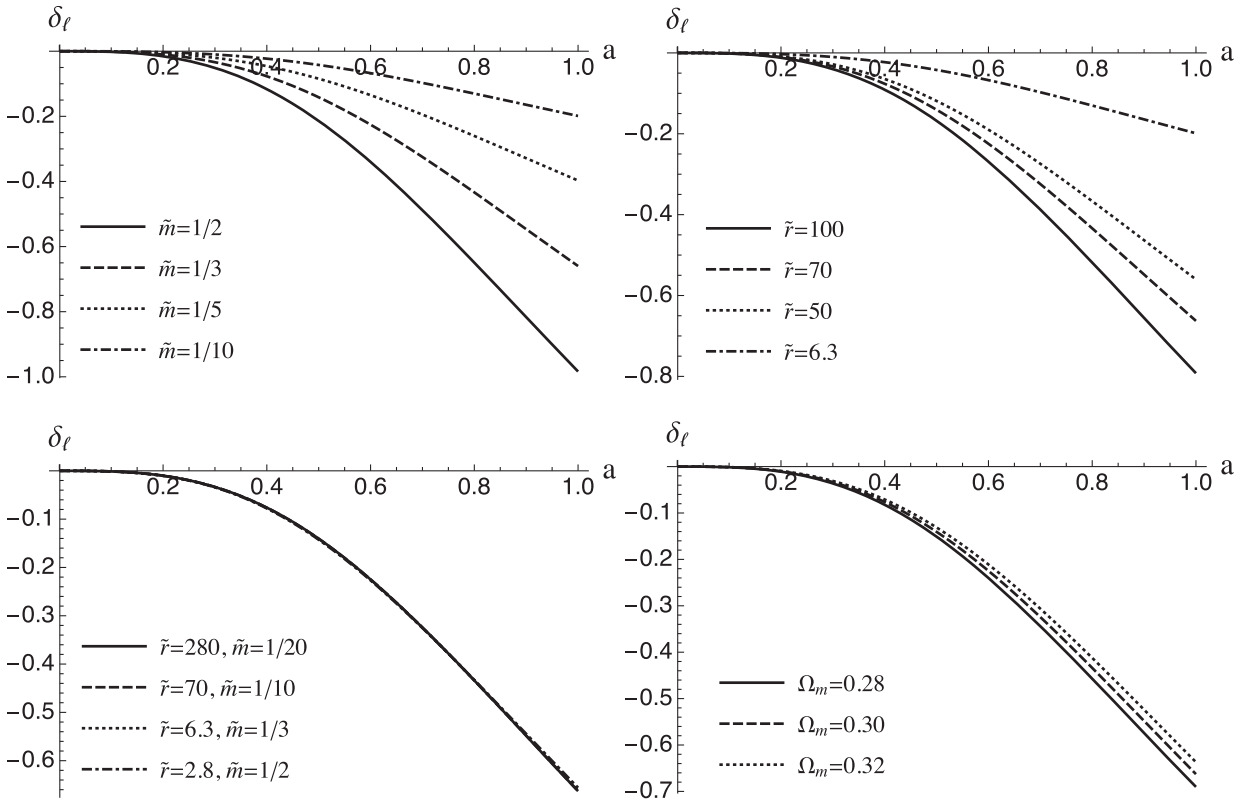

FIG. 10. Numerical solutions for the matter perturbation δ_ℓ. The upper left and upper right panels demonstrate the dependence of δ_ℓ on $\tilde{m}$ and $\tilde{r}$, respectively. The lower left panel assumes the same value of $\Omega_m = 0.3$, while the lower right panel assumes slightly different values of Ω_m, where $\tilde{r} = 70$ and $\tilde{m} = 1/10$ are fixed. The lower panels show that δ_ℓ will be almost independent of $\tilde{r}$ or $\tilde{m}$ values, as long as they satisfy Eq. (46).

δ_ℓ, which is demonstrated in the upper left panel and the upper right panel of Fig. 10, respectively. However, for natural choices mimicking the standard ΛCDM scenario, satisfying Eq. (46), the coefficient $F \approx 1$ holds; hence, we have $\delta_\ell \simeq -(27/22)(1-\Omega_m)\tilde{t}^2$, which explains the behavior of δ_ℓ in the lower panels of Fig. 10.

IV. APPLICATIONS

In this section, we consider two applications of our model for CMB temperature fluctuations and luminosity distance. The first is the integrated Sachs-Wolfe (ISW) effect [48,49]. Some aspects of this effect were investigated in a previous paper [48], which relies on the statistical argument based on the two-point correlation function. We revisit this problem by applying the formulations developed in the present study. The second is the impact on the luminosity distances, which is related to the observations of SNe Ia.

As noted following the definition of ϕ, Eq. (4), ϵ_ℓ was introduced to explicitly express the order of perturbations that are small, and was related to the coordinates we choose to define the multipoles of the perturbations in Eqs. (2)–(6). These amplitudes of perturbations will be taken unity, that is, $\epsilon_\ell \sim \mathcal{D}_{(\ell m)} \equiv 1$ [see also Eqs. (65), (66), (69), and (70)], for the purpose of numerical evaluation, where most importantly we are interested in the evolution of the perturbations. These amplitudes of the perturbations will be constrained by reintroducing other parameters ε_1 and ε_2 when comparing with the actual CMB multipoles observed.

A. CMB temperature fluctuations

Through the ISW effect, the perturbations to the metric caused by the large-scale inhomogeneities of the dark energy ϕ affect the observations of the CMB anisotropies. By using the relation between the comoving distance and the conformal time on the photon's path on the background, $\chi = \eta_0 - \eta$, we can evaluate the ISW effect on the temperature fluctuations of the CMB as

$$\begin{aligned}\frac{\Delta T}{T} &\simeq 2\int_{\eta_d}^{\eta_0} \mathrm{d}\eta \left(\frac{\partial \Psi(\eta,\chi,\theta,\varphi)}{\partial\eta}\right)\Big|_{\chi=\eta_0-\eta} \\ &= 2\int_{\eta_d}^{\eta_0} \mathrm{d}\eta \left(\sum_{m=1}^{3}\frac{\partial \Psi_{1(m)}(\eta)}{\partial\eta} P_i^{(m)} x^i + \sum_{m=1}^{5}\frac{\partial \Psi_{2(m)}(\eta)}{\partial\eta} P_{ij}^{(m)} x^i x^j\right)\Big|_{\chi=\eta_0-\eta} \\ &= 2\int_{\eta_d}^{\eta_0} \mathrm{d}\eta \left(\frac{\partial \Psi_{1(m)}(\eta)}{\partial\eta} \sum_{m=1}^{3} P_i^{(m)} x^i\right)\Big|_{\chi=\eta_0-\eta} + 2\int_{\eta_d}^{\eta_0} \mathrm{d}\eta \left(\frac{\partial \Psi_{2(m)}(\eta)}{\partial\eta} \sum_{m=1}^{5} P_{ij}^{(m)} x^i x^j\right)\Big|_{\chi=\eta_0-\eta}, \end{aligned} \tag{75}$$

where η_d denotes the era of the photon decoupling. In the last line of Eq. (75), we used the Einstein summation convention with respect to the index of m. We note that $\Psi_{\ell(m)}$, which are denoted as Ψ_ℓ with the index m omitted in the previous section for simplicity, are only functions of the conformal time η. It can also be confirmed that the matrices P_{ij}^m and P_i^m introduced in Sec. II are related to the real basis spherical harmonics $Y_\ell^m(\theta,\varphi)$ (see Appendix A). By utilizing the relation in Eqs. (A8) and (A9), it follows that

$$\begin{aligned}\frac{\Delta T}{T} &= 2\sum_m \int_{\eta_d}^{\eta_0} \mathrm{d}\eta \left(\frac{\partial \Psi_{1(m)}}{\partial\eta}\chi Y_{\ell=1}^{(m)}(\theta,\varphi)\right)\Big|_{\chi=\eta_0-\eta} \\ &\quad + 2\sum_m \int_{\eta_d}^{\eta_0} \mathrm{d}\eta \left(\frac{\partial \Psi_{2(m)}}{\partial\eta}\chi^2 Y_{\ell=2}^{(m)}(\theta,\varphi)\right)\Big|_{\chi=\eta_0-\eta} \\ &\equiv 2\sum_{\ell=1}^{2}\sum_{m=1}^{2\ell+1} Q_{\ell(m)} Y_\ell^{(m)}(\theta,\varphi), \end{aligned} \tag{76}$$

with

$$Q_{\ell(m)} \equiv \int_{\eta_d}^{\eta_0} \mathrm{d}\eta (\eta_0-\eta)^\ell \frac{\partial \Psi_{\ell(m)}}{\partial\eta} \tag{77}$$

defined. Because we have obtained the evolution of the perturbation $\Psi_{\ell(m)}$ in the previous numerical solution in Sec. III, $Q_{\ell(m)}$ can be numerically evaluated.

On the other hand, the angular two-point correlation function can be written in multipole expansion as [56]

$$\left\langle \frac{\Delta T}{T}(\boldsymbol{\gamma}) \frac{\Delta T}{T}(\boldsymbol{\gamma}') \right\rangle = \sum_\ell \frac{2\ell+1}{4\pi} C_\ell P_\ell(\cos\theta), \tag{78}$$

where $\boldsymbol{\gamma}$ and $\boldsymbol{\gamma}'$ represent different unit line-of-sight directions with included angle θ, i.e., $\boldsymbol{\gamma}\cdot\boldsymbol{\gamma}' = \cos\theta$. The angular power spectrum C_ℓ is defined by the ensemble of squared expansion coefficients as follows:

$$C_\ell \equiv \frac{\sum_{m=1}^{2\ell+1} |A_{\ell m}|^2}{2\ell+1}, \tag{79}$$

where the coefficients are defined by

$$\frac{\Delta T}{T} = \sum_\ell \sum_{m=1}^{2\ell+1} A_{\ell m} Y_\ell^{(m)}(\theta,\varphi). \tag{80}$$

Here we used $1 \le m \le 2\ell+1$ to denote the magnetic quantum number. By comparing Eq. (76) with (80), we find that

$$A_{\ell m} = 2Q_{\ell(m)} = 2\left(\int_{\eta_d}^{\eta_0} \mathrm{d}\eta(\eta_0-\eta)^\ell \frac{\partial \Psi_{\ell(m)}}{\partial \eta}\right). \quad (81)$$

A constraint on our model from the observational CMB power spectrum is $C_\ell \le C_\ell^{\rm obs}$, which means that the contribution of the large-scale mode perturbations to the CMB power spectrum multipoles should not exceed what is actually observed, because there may be other sources contributing to the anisotropies, as long as cancellations do not occur. Consequently, we have two constraints from the $\ell = 1$ dipole and the $\ell = 2$ quadrupole, respectively, as

$$\frac{4\sum_{m=1}^{2\ell+1} Q_{\ell(m)}^2}{2\ell+1} \le C_\ell^{\rm obs}. \quad (82)$$

Thanks to the Planck Legacy Archive,[1] we can apply the upper limit of the observational data as $C_1^{\rm obs} < 6.3\times 10^{-6}$ and $C_2^{\rm obs} < (2\pi/6)\times(1.0\times 10^{-10})$ to put constraints on the amplitudes of the perturbations.

For example, for both parameter sets $(\tilde{r}=70, \tilde{m}=1/10)$ and $(\tilde{r}=6.3, \tilde{m}=1/3)$, or, more generally, for models close to ΛCDM sets labeled with Nos. (1), (2), (7), and (8) in Table I, where the condition in Eq. (46) is satisfied, the calculations on $Q_{1(m)}$ and $Q_{2(m)}$ give consistent results as

$$Q_{1(m)} = -1.1\times 10^{-1}\mathcal{D}_{(1m)}, \quad (83)$$

$$Q_{2(m)} = -9.0\times 10^{-2}\mathcal{D}_{(2m)}, \quad (84)$$

where the amplitude of the perturbations for each mode $\mathcal{D}_{(\ell m)}$ is recovered, which lead to the following constraints:

$$\varepsilon_1 \equiv \left[\frac{\sum_{m=1}^{2\ell+1}\mathcal{D}_{(1m)}^2}{2\ell+1}\right]^{1/2} \le 1.2\times 10^{-2}, \quad (85)$$

$$\varepsilon_2 \equiv \left[\frac{\sum_{m=1}^{2\ell+1}\mathcal{D}_{(2m)}^2}{2\ell+1}\right]^{1/2} \le 5.7\times 10^{-5}, \quad (86)$$

because both parameter sets mimic the cosmology close to a ΛCDM model to yield the observational constraints safely. We also present numerical evaluations with different parameter choices in Table I.

B. Perturbations to light propagation and luminosity distance

Following Refs. [53,57], as we have solved the metric perturbations Ψ_ℓ associated with large-scale fluctuations of the dark energy, we can evaluate the perturbation to the luminosity distance introduced by the inhomogeneities of the dark energy by considering the metric perturbations formulated previously. The relative perturbations of the luminosity distance in an inhomogeneous universe is given as [52,53]

$$I \equiv \frac{\delta d_L}{d_L} = \int_0^{\lambda_s} \mathrm{d}\lambda \frac{\lambda}{\lambda_s}(\lambda-\lambda_s)\left(\Delta^{(3)}\Psi - \left(\ddot{\Psi} + 2\frac{\mathrm{d}\dot{\Psi}}{\mathrm{d}\lambda}\right)\right), \quad (87)$$

where $\dot{\Psi} \equiv \frac{\partial\Psi(\eta,\chi)}{\partial\eta}$, and we have assumed a spatially flat universe. The traceless property of matrices $P_{ij}^{(m)}$ defined by Eq. (2) in Ψ ensures that $\Delta^{(3)}\Psi = 0$ [see Eq. (A10)].

For the term containing differentiation with respect to the propagation parameter λ, we may write

$$\frac{\mathrm{d}}{\mathrm{d}\lambda} = \frac{\mathrm{d}\eta}{\mathrm{d}\lambda}\frac{\partial}{\partial\eta} + \frac{\mathrm{d}\chi}{\mathrm{d}\lambda}\frac{\partial}{\partial\chi}. \quad (88)$$

Here, we may take the parameter λ as the comoving distance χ; hence, $\lambda \equiv \chi = \eta_0 - \eta$ and $\lambda_s \equiv \chi_s = \eta_0 - \eta_s$ with an arbitrary light source indicated by subscript s. Thus, we have

$$I = \int_0^{\chi_s} \mathrm{d}\chi \frac{\chi}{\chi_s}(\chi-\chi_s)\left(\ddot{\Psi} - 2\frac{\partial\dot{\Psi}}{\partial\chi}\right). \quad (89)$$

Using a procedure similar to that used to transform Eqs. (75) and (76), with the definition of Ψ in Eq. (2) and Eqs. (A8)–(A9), we can rewrite I as

$$\begin{aligned} I &= \int_0^{\chi_s} \mathrm{d}\chi(\chi-\chi_s)\frac{\chi}{\chi_s}\left[\left(\ddot{\Psi}_{\ell(m)} - 2\dot{\Psi}_{\ell(m)}\frac{\partial}{\partial\chi}\right)\right. \\ &\quad \left.\times\left(\sum_{m=1}^{3}\chi Y_{\ell=1}^{(m)}(\theta,\varphi) + \sum_{m=1}^{5}\chi^2 Y_{\ell=2}^{(m)}(\theta,\varphi)\right)\right] \\ &\equiv \sum_{\ell=1}^{2}\sum_{m=1}^{2\ell+1} S_{\ell(m)} Y_\ell^{(m)}(\theta,\varphi), \end{aligned} \quad (90)$$

with the integral defined as

$$S_{\ell(m)} \equiv \int_0^{\chi_s} \mathrm{d}\chi \frac{\chi-\chi_s}{\chi_s}(\chi^{\ell+1}\ddot{\Psi}_{\ell(m)} - 2\ell\chi^\ell\dot{\Psi}_{\ell(m)}). \quad (91)$$

It is worth reminding the reader again that $\Psi_{\ell(m)}(\eta)$ is only a function of η. $S_{\ell(m)}$ is the quantity that reflects the impact of accumulative corrections on the luminosity distance by the inhomogeneities of the dark energy, which can be evaluated numerically.

We evaluate $S_{\ell(m)}$ due to the perturbation of Ψ caused by dark energy inhomogeneity as a function of a or the

[1]Based on observations obtained with Planck (http://www.esa.int/Planck), an ESA science mission with instruments and contributions directly funded by ESA Member States, NASA, and Canada.

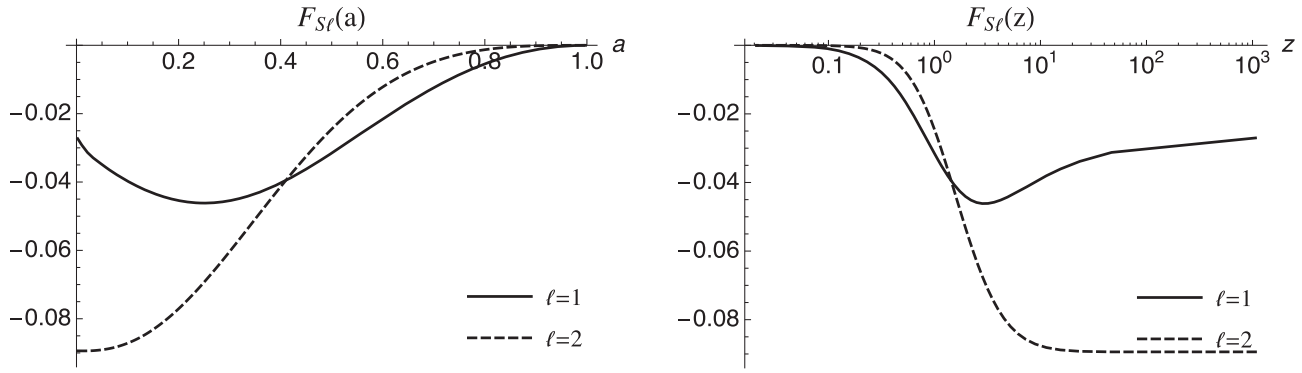

FIG. 11. Multipole components of the perturbations to the luminosity distance defined as $F_{S\ell(m)}(a;z)$ as a function of scale factor a (left panel) and redshift z (right panel). In each panel, the solid curve is the dipole, $\ell = 1$, and the dashed curve is the quadrupole $\ell = 2$. Here we adopted model No. (1) in Table I.

cosmological redshift z, corresponding to the light sources from different epochs,

$$S_{\ell(m)}(a) = F_{S\ell(m)}(a)\mathcal{D}_{(\ell m)}. \tag{92}$$

Then we have

$$F_{S\ell(m)}(a) \equiv \int_{\eta_0}^{\eta_s(a)} \mathrm{d}\eta \left((\eta_0 - \eta)^{\ell+1} \frac{\partial^2 \Psi_{\ell(m)}}{\partial \eta^2} - 2\ell(\eta_0 - \eta)^{\ell} \frac{\partial \Psi_{\ell(m)}}{\partial \eta} \right) \frac{\eta - \eta_s(a)}{\eta_0 - \eta_s(a)}, \tag{93}$$

in a more explicit manner for numerical evaluation with respect to scale factor a using a_1 as the variable of integration,

$$F_{S\ell(m)}(a) = -\int_a^1 \mathrm{d}a_1 \left[(\eta_0 - \eta(a_1))^{\ell+1} \frac{\partial}{\partial a_1} \left(a_1^2 H(a_1) \frac{\partial \Psi_{\ell(m)}}{\partial a_1} \right) - 2\ell(\eta_0 - \eta(a_1))^{\ell} \frac{\partial \Psi_{\ell(m)}}{\partial a_1} \right] \frac{\eta(a_1) - \eta_s(a)}{\eta_0 - \eta_s(a)}. \tag{94}$$

We notice that $F_{S\ell(m)}(a)$ does not increase or decrease monotonically, whose typical behaviors are illustrated as a function of a or z in Fig. 11. The scale factor is related to the cosmological redshift by $z = a^{-1} - 1$, which is used to convert each other.

Because we have solved for the system as functions of the scale factor a in Sec. III, $\Psi_\ell(a)$, $\eta(a)$, and $H(a)$, and the particle horizon η_0 are already known for the given parameters $\tilde{r}$ and $\tilde{m}$. If necessary, we can also transform these quantities using the conformal time η as an independent variable (see Appendix F). On the other hand, we put constraints on ε_1 and ε_2 in Sec. IV A; thus, we can evaluate the modification to the luminosity distance I with Eq. (90) by numerically evaluating $S_{\ell(m)}$ with the constraint Eqs. (85) and (86). Our numerical results $F_{S\ell(m)}$ are shown in Fig. 11 as a function of a (left panel) and z (right panel), respectively. Our results with different parameters can be found in Table I. We evaluated $F_{S\ell(m)}(a)$ at $a = 0.25$, which corresponds to $z = 3$.

We estimate the multipole components of I as

$$I_\ell \equiv \sum_{m=1}^{2\ell+1} S_{\ell(m)} \sim (2\ell + 1) S_{\ell(m)}. \tag{95}$$

Allowed values of $\mathcal{D}_{(\ell m)} \sim \mathcal{O}(\varepsilon_\ell)$ ($\ell = 1, 2$) are found in Sec. IV A [see Eqs. (85) and (86)]; e.g., with $\varepsilon_1 < 1.2 \times 10^{-2}$ and $\varepsilon_2 < 5.7 \times 10^{-5}$, we can evaluate the modification to the luminosity distance caused by large-scale vector modes using Eq. (90) that the magnitude of the correction caused by the $\ell = 1$ component is $\mathcal{O}(10^{-3})$, whereas it is $\mathcal{O}(10^{-5})$ for the $\ell = 2$ component. We have the consistent results of modification to the luminosity distance I_ℓ as

$$I_{\ell=1} \simeq -1.6 \times 10^{-3}, \tag{96}$$

$$I_{\ell=2} \simeq -2.0 \times 10^{-5}, \tag{97}$$

at the redshift $z = 3$ for all models in Table I.

V. DISCUSSIONS AND CONCLUSIONS

We formulated a cosmological model with inhomogeneous dark energy sourced from a dynamical scalar field with extremely large-scale fluctuations, by handling them as cosmological perturbations to a homogeneous background to focus on a local observable universe. This model is capable of reproducing an observable universe that mimics the ΛCDM flat universe favored by the observations but with inhomogeneity and anisotropy of small amplitudes on very large scales. We investigated the basic equations governing the evolution of the universe for the background and perturbations, and presented the numerical solutions for these equations by choosing appropriate

parameters that reproduce cosmological models close to the ΛCDM universe. As the examples for the application of the results, we investigated the impact of the extremely large-scale inhomogeneity of the dark energy on the cosmological observations in the late-time universe, where dark energy becomes important for background evolution.

In our numerical evaluations, we chose the parameters of the models close to the ΛCDM model, for example, $(\tilde{r} = 70, \tilde{m} = 1/10)$ and $(\tilde{r} = 6.3, \tilde{m} = 1/3)$, which satisfies the condition in Eq. (46). However, the prediction of the models is robust for the different choices of the parameters $(\tilde{r}, \tilde{m})$, as shown in Table I in Sec. III. We also showed that slight changes in the values of Ω_m do not alter the results. The observational constraints on cosmological parameters allow deviation from the standard ΛCDM scenario to some extent [29,30], potentially suggesting that dynamical quintessence models for dark energy EoS are favored [58]. Hence it is interesting to investigate constraints on the parameter space consistent with these observations.

Using numerical solutions, we focused our investigation on the impact of the large-scale inhomogeneities of the dark energy on the large angular anisotropies in the CMB temperature map and in the luminosity distance. The time variations of the metric perturbations give rise to the ISW effect, which affects the temperature anisotropies. In contrast to previous work [48], we investigated the multipole spectrum in the spatially flat universe using numerical solutions without approximations. We obtained the constraints Eqs. (85) and (86) on the amplitude of the models from the observational data. The contribution from the large-scale inhomogeneities of the dark energy on the dipole of the CMB temperature power spectrum may partly account for the anomalies in the dipole and low multipoles of the CMB power spectra [34,56].

The inhomogeneities of the dark energy affect the cosmic distance, which may impact the observations of SNe Ia and BAO measurements. We used Eq. (87), according to Refs. [53,57], for evaluation of these parts. Our numerical calculations showed that the relative correction to the luminosity distance could be $\mathcal{O}(10^{-3})$ for the dipole and $\mathcal{O}(10^{-5})$ for the quadrupole components. For general parameter choices in Table I, these corrections seem too small to resolve the Hubble tension, which is becoming increasingly conspicuous between measurements via CMB and via standard candles such as SNe Ia [59–61], as addressed in Sec. I. In a potentially related work Ref. [62] as a comparison with our model, the authors attempted to ease the H_0 tension by introducing local inhomogeneities from the coupling of a chameleon dark energy model with dark matter. However, comprehensive analyses, including wide ranges of the model parameters and the various observational results taking systematics into account, will be interesting [58,63,64]. Especially, the future progress of the gravitational wave observations with associative electromagnetic observations will be promising to provide with a standard siren [65–68].

Our model presented here is a possible dark energy model predicting the anisotropic expansion rate or anisotropic dark energy density and equation of state. Using the solutions in the present paper, we can realize the dynamical dark energy models with the inhomogeneous density on the large scales on the smooth background of the local universe. Another application of this inhomogeneous model may be to investigate its prediction on the structure formation, especially on large scales, though it is beyond the scope of this paper. Potentially related to this aspect, Refs. [69,70] investigated the impacts of different classes of dark energy models on matter clustering, which may help to discriminate our model from other models in the context of matter clustering. The inhomogeneous dark energy model will be interesting from the viewpoint that it is potentially verifiable/falsifiable by the ongoing/planned data release of existing observations and future generation observations [for example, DES, DESI, LSST [71], Euclid [72], and Roman Space Telescope (formerly known as WFIRST) [73], cf. [31]]. Additionally, the neutral hydrogen cosmology from the 21 cm spectrum survey planned by SKA [74] may link BAO with redshift-space distortions and add up to a better understanding of dark energy. The future data of these surveys may help to test the inhomogeneous properties of the dark energy.

The work in the present paper is inspired by a previous work [48], in which large-scale dark energy perturbations are generated by the quantum fluctuations of a scalar field according to an open-inflation scenario. The original model predicts a cosmological model with negative spatial curvature. However, in the present study, we considered a spatially flat universe $\Omega_K = 0$; therefore, the origin of the scalar field as the candidate for dark energy in our model is a subject to be discussed further. Recently, ultralight scalar fields such as axionlike particles have attracted great interest as cosmological candidates for dark energy and dark matter [27], linked with the strong CP problem and motivated by the string axiverse and the swampland conjectures [20,21,24,25,75,76]. Exploring the possibility to generate the initial conditions necessary for a scalar field in our model could be interesting within the framework of these scenarios in future investigations.

ACKNOWLEDGMENTS

This work was supported by Grant-in-Aid for JSPS fellows Grant No. JP20J13640 (Y. N.), and MEXT/JSPS KAKENHI Grants No. 15H05895, No. 16H03977, No. 17K05444, No. 17H06359 (K. Y.). We thank K. Yamashita, Y. Sugiyama, Y. Kojima, N. Okabe, A. Naruko, and M. Sasaki for fruitful discussions and helpful comments. We are also grateful for anonymous referees, whose comments improved the quality of the manuscript.

APPENDIX A: MULTIPOLE EXPANSION MATRICES

The matrices appearing in the definitions of the perturbations in Sec. II A, $P_i^{(m)}$ are simply written as

$$P_i^{(m=1)} = \sqrt{\frac{3}{4\pi}}\begin{pmatrix}1\\0\\0\end{pmatrix}, \qquad P_i^{(m=2)} = \sqrt{\frac{3}{4\pi}}\begin{pmatrix}0\\1\\0\end{pmatrix},$$
$$P_i^{(m=3)} = \sqrt{\frac{3}{4\pi}}\begin{pmatrix}0\\0\\1\end{pmatrix}, \tag{A1}$$

while $P_{ij}^{(m)}$ are traceless matrices related to the multipole expansion of the perturbations and are listed as follows:

$$P_{ij}^{(m=1)} = \sqrt{\frac{15}{16\pi}}\begin{pmatrix}0&1&0\\1&0&0\\0&0&0\end{pmatrix}, \tag{A2}$$

$$P_{ij}^{(m=2)} = \sqrt{\frac{15}{16\pi}}\begin{pmatrix}0&0&0\\0&0&1\\0&1&0\end{pmatrix}, \tag{A3}$$

$$P_{ij}^{(m=3)} = \sqrt{\frac{15}{16\pi}}\begin{pmatrix}0&0&1\\0&0&0\\1&0&0\end{pmatrix}, \tag{A4}$$

$$P_{ij}^{(m=4)} = \sqrt{\frac{15}{16\pi}}\begin{pmatrix}1&0&0\\0&-1&0\\0&0&0\end{pmatrix}, \tag{A5}$$

$$P_{ij}^{(m=5)} = \sqrt{\frac{15}{16\pi}}\begin{pmatrix}-1&0&0\\0&-1&0\\0&0&2\end{pmatrix}. \tag{A6}$$

Equations (2)–(4) are due to the multipole expansion of the inhomogeneous perturbations under the real spherical harmonics: in the space up to $\ell = 2$, the quadrupole component, with the $\ell = 0$ component representing the homogeneous background as the monopole.

Using θ and φ to denote the polar and azimuthal angles in the spherical coordinates, respectively, taking the spatial basis

$$x^1 = \chi\sin\theta\cos\varphi,$$
$$x^2 = \chi\sin\theta\sin\varphi,$$
$$x^3 = \chi\cos\theta, \tag{A7}$$

the relation between these matrices and the spherical harmonics can be understood as

$$Y^{(m)}_{\ell=1}(\theta,\varphi) \equiv P_i^{(m)}x^i/\chi, \tag{A8}$$

$$Y^{(m)}_{\ell=2}(\theta,\varphi) \equiv P_{ij}^{(m)}x^ix^j/\chi^2, \tag{A9}$$

with integer $m \in [1, 2\ell+1]$ instead of $m \in [-\ell, \ell]$, corresponding to the three matrices for $\ell = 1$ and five matrices for $\ell = 2$ previously.

Note that the traceless property for the matrices corresponds to the conclusion that the large-scale modes make no source term contribution additional to the scalar modes as its Laplacian vanishes

$$\begin{aligned}\Delta^{(3)}\Psi = \nabla^2\Psi &= \Psi_{1(m)}\nabla^2P_i^{(m)}x^i + \Psi_{2(m)}\nabla^2P_{ij}^{(m)}x^ix^j\\ &= 0 + \mathrm{Tr}P_{ij}^{(m)}\Psi_{2(m)}\nabla^2\chi^2\\ &= 0.\end{aligned} \tag{A10}$$

APPENDIX B: THE FLUID EQUATION CONSISTENCY

Starting from Eq. (17), if we refine $\mathcal{V}_\ell$ with respect to V_ℓ as

$$\mathcal{V}_\ell \equiv \frac{k}{a}V_\ell, \tag{B1}$$

with k denoting the wave number of the perturbations, we will have

$$\dot{V_\ell} - a\Psi_\ell = \frac{\dot{a}\mathcal{V}_\ell + a\dot{\mathcal{V}}_\ell}{k} - a\Psi_\ell = 0, \tag{B2}$$

and hence

$$\dot{\mathcal{V}}_\ell + \frac{\dot{a}}{a}\mathcal{V}_\ell - k\Psi_\ell = 0, \tag{B3}$$

which is consistent with Eq. (26) in Ref. [48].

APPENDIX C: ADDITIONAL DETAILS FOR THE BACKGROUND EVOLUTION

In this Appendix, we present more details for preparing the background equations for numerical solutions with the initial conditions.

1. As functions of dimensionless time $\tilde{t}$

We have introduced the dimensionless ordinary differential equations of the background using $\tilde{t}$ as an independent variable as

$$\tilde{r}\tilde{m}^2\tilde{\phi}_0^2(\tilde{t}) + \tilde{r}\left(\frac{\mathrm{d}\tilde{\phi}_0}{\mathrm{d}\tilde{t}}\right)^2 + \Omega_m a^{-3} = \left(\frac{1}{a}\frac{\mathrm{d}a}{\mathrm{d}\tilde{t}}\right)^2,$$
$$\frac{\mathrm{d}^2\tilde{\phi}_0}{\mathrm{d}\tilde{t}^2} + 3\frac{1}{a}\frac{\mathrm{d}a}{\mathrm{d}\tilde{t}}\frac{\mathrm{d}\tilde{\phi}_0}{\mathrm{d}\tilde{t}} + \tilde{m}^2\tilde{\phi}_0 = 0,$$

where H_0 is the Hubble constant and $\overline{\phi}_0$ is a constant related to the initial value of ϕ_0.

It is worth noting that according to the definitions in Eqs. (33)–(36), there are 2 degrees of freedom for the parameters $\tilde{m}$ and $\tilde{r}$, to specify the mass and energy scale of the dark energy field ϕ, respectively. The unknown component in our model, dark energy ϕ, can be fundamentally characterized by two parameters. One is the shape of its potential $V(\phi) = m_\phi^2\phi^2/2$, and the other is the initial value in our universe, while the properties of the other component (e.g., matter) are considered as known under the standard cosmological model.

To focus on the solution, in search of initial conditions and the analytic approximations in the limit $a \ll 1$, Eq. (38) approaches

$$\left(\frac{1}{a}\frac{\mathrm{d}a}{\mathrm{d}\tilde{t}}\right)^2 = \Omega_m a^{-3}, \tag{C1}$$

which has the solution

$$\tilde{t} = \frac{2}{3}\frac{a^{\frac{3}{2}}}{\sqrt{\Omega_m}} \quad \text{or} \quad a = \left(\frac{9}{4}\Omega_m\right)^{\frac{1}{3}}\tilde{t}^{\frac{2}{3}} \tag{C2}$$

as an analytic approximation in the limit $a \ll 1$.

Inserting this into Eq. (39) gives

$$\frac{\mathrm{d}^2\tilde{\phi}_0}{\mathrm{d}\tilde{t}^2} + 2\frac{1}{\tilde{t}}\left(\frac{\mathrm{d}\tilde{\phi}_0}{\mathrm{d}\tilde{t}}\right) + \widetilde{m_\phi^2}\tilde{\phi}_0 = 0, \tag{C3}$$

which has the general solution

$$\tilde{\phi}_0(\tilde{t}) = C_1\frac{\sin(\tilde{m}\,\tilde{t})}{\tilde{m}\,\tilde{t}} + C_2\frac{\cos(\tilde{m}\,\tilde{t})}{\tilde{m}\,\tilde{t}}. \tag{C4}$$

The cosine part diverges in the limit $a \ll 1$ to be abandoned; hence, we write

$$\tilde{\phi}_0(\tilde{t}) = C_1\frac{\sin(\tilde{m}\,\tilde{t})}{\tilde{m}\,\tilde{t}}, \tag{C5}$$

which imposes the initial condition

$$\tilde{\phi}_0(\tilde{t}\to 0) = \lim_{\tilde{t}\to 0} C_1\frac{\sin(\tilde{m}\,\tilde{t})}{\tilde{m}\,\tilde{t}} = C_1. \tag{C6}$$

However, the initial value of $\tilde{\phi}_0(\tilde{t}\to 0) = C_1$ is not self-evident and should be determined in association with the dark energy density of the present epoch inferred from observations. We have the constraint from the present Hubble rate to fix $\tilde{t}_0$ by definitions

$$a(\tilde{t}_0) = a(H_0 t_0) \equiv 1,$$
$$H(\tilde{t}_0) = H(H_0 t_0) \equiv H_0.$$

Inserting this into Eq. (38) actually gives Eq. (45),

$$1 - \Omega_m = \tilde{r}\tilde{m}^2(\tilde{\phi}_0|_{\tilde{t}=\tilde{t}_0})^2 + \tilde{r}\left(\frac{\mathrm{d}\tilde{\phi}_0}{\mathrm{d}\tilde{t}}\bigg|_{\tilde{t}=\tilde{t}_0}\right)^2.$$

Equation (45) is the necessary condition for specifying the dark energy density observed today when solving the background equations. Together with Eqs. (38) and (39), the system is now prepared for numerical evaluation to obtain the evolution of $a(\tilde{t})$ and $\tilde{\phi}_0(\tilde{t})$. As we are mainly interested in the late-time evolution here, we can determine the initial value for independent variables $\tilde{t}$ or a (to be discussed later) manually as a typical value; for example, $a_i = a_d \approx 1/1100$ at the photon decoupling off the last scattering, by use of Eq. (C2). These solutions determine the background evolution that we rely on to solve the perturbation equations.

It is worth mentioning that Eq. (45) also provides a baseline for choosing the parameters $\tilde{m}$ and $\tilde{r}$ from the various parameter spaces. In the case of the cosmological constant Λ, $\mathrm{d}\tilde{\phi}_0/\mathrm{d}\tilde{t}$ is always small, leaving

$$1 - \Omega_m = \tilde{r}\tilde{m}^2(\tilde{\phi}_0|_{\tilde{t}=\tilde{t}_0})^2. \tag{C7}$$

Thus, if we take the dimensionless field in the present epoch normalized as $\tilde{\phi}_0(\tilde{t} = \tilde{t}_0) \sim \mathcal{O}(1) \equiv 1$, we will have a special case for the choice of parameters approximating the ΛCDM model presented in Eq. (46) that $\tilde{r}\tilde{m}^2 \simeq 1 - \Omega_m$.

2. As functions of scale factor a

Because the scale factor a can be chosen as a time-evolution parameter instead of the dimensionless time $\tilde{t}$, as a double-check for the previous subsection, we can write out the dimensionless equations for $\tilde{\phi}_0$ and $\tilde{H}(a)$ as functions of the scale factor a. Recall that the superscript $'$ means derivative with respect to scale factor a. By inserting Eq. (42) into Eq. (41), we obtain the background equation to be solved in the form

$$\tilde{m}^2a^2\tilde{\phi}_0(1 - \tilde{r}a^2\tilde{\phi}_0'^2) + \tilde{m}^2\tilde{r}a^3\tilde{\phi}_0^2(4\tilde{\phi}_0' - 3\tilde{r}a^2\tilde{\phi}_0'^3 + a\tilde{\phi}_0'')$$
$$+ \frac{\Omega_m}{2}(5\tilde{\phi}_0' - 3\tilde{r}a^2\tilde{\phi}_0'^3 + 2a\tilde{\phi}_0'') = 0, \tag{C8}$$

where an initial condition for $\tilde{\phi}_0(a)$ is necessary. After solving $\tilde{\phi}_0(a)$, we can obtain $\tilde{H}(a)$ from Eq. (42).

For the initial conditions, we consider the analytic approximations. When $a \ll 1$, Eq. (42) simply approaches

$$\tilde{H} = \sqrt{\Omega_m} a^{-3/2}. \tag{C9}$$

Inserting this into Eq. (41) and simplifying will lead to

$$a\tilde{\phi}_0'' + \frac{5}{2}\tilde{\phi}_0' + \tilde{m}^2 a^2 \Omega_m^{-1} \tilde{\phi}_0 = 0, \tag{C10}$$

which can be solved analytically as

$$\tilde{\phi}_0(a) = C_1 \frac{3\sqrt{\Omega_m}}{2\tilde{m}a^{3/2}} \sin\left(\frac{2\tilde{m}a^{3/2}}{3\sqrt{\Omega_m}}\right), \tag{C11}$$

which is identical to that in Eq. (C5) by recalling Eq. (C2). Then we are able to infer

$$\tilde{\phi}_0(a \to 0) = C_1, \tag{C12}$$

$$\tilde{\phi}_0{}'(a \to 0) = 0, \tag{C13}$$

are the appropriate initial conditions for the system, which are consistent with the equations using dimensionless time $\tilde{t}$ as the independent variable. Now the background equations can be solved numerically.

APPENDIX D: DARK ENERGY EoS AS A FUNCTION OF THE SCALE FACTOR a

Following Eq. (12), we have

$$\begin{aligned} \omega_\phi &= -\frac{m_\phi^2 a^2 \phi^2 - \dot{\phi}^2}{m_\phi^2 a^2 \phi^2 + \dot{\phi}^2} \\ &= -1 + \frac{2}{m_\phi^2 a^2 (\phi/\dot{\phi})^2 + 1} \\ &\equiv -1 + 2W(a), \end{aligned} \tag{D1}$$

where $'$ denotes the derivative of the scale factor a, $' \equiv \partial/\partial a$, where

$$W(a) \equiv \frac{1}{m_\phi^2 a^2 (\phi/\dot{\phi})^2 + 1} = \frac{a^2}{(m_\phi/H)^2 (\phi/\phi')^2 + a^2}. \tag{D2}$$

At the background level assuming $\tilde{\phi} \simeq \tilde{\phi}_0$, we can further write

$$W(a) \simeq \frac{\tilde{\phi}_0'^2 a^2 \tilde{H}^2}{\tilde{m}^2 \tilde{\phi}_0^2 + \tilde{\phi}_0'^2 a^2 \tilde{H}^2}. \tag{D3}$$

Recall that $\tilde{H}(a)$ is defined in Eq. (42), which depends on the values of $\tilde{r}$, $\tilde{m}$, and Ω_m. Because $\tilde{m}^2$ is typically small in our model, using Eq. (42) and expanding to the order of $\mathcal{O}(\tilde{m}^2)$, we have

$$\begin{aligned} W(a) &\simeq 1 - \frac{a\tilde{m}^2}{\Omega_m}\left(\frac{\tilde{\phi}_0^2}{\tilde{\phi}_0'^2}\right)(1 - \tilde{r}a^2\tilde{\phi}_0'^2) \\ &\simeq 1 - \frac{a\tilde{m}^2}{\Omega_m}\left(\frac{\tilde{\phi}_0^2(a)}{\tilde{\phi}_0'^2(a)}\right), \end{aligned} \tag{D4}$$

which can be numerically evaluated with $\tilde{\phi}_0(a)$ and $\tilde{\phi}_0'(a)$ as demonstrated in Sec. III. The second line stands because $a^2\tilde{\phi}_0'^2$ is small and negligible for $0 < a < 1$ in almost all cases. Then, we can understand that $\tilde{r}$ hardly affects the background EoS of the dark energy.

Although slightly complicated in its explicit form, Eqs. (D1)–(D4) can be considered as a natural extension of the CPL parametrization of the dark energy EoS [50,51]. This is a manifestation of how the behaviors of the EoS of dark energy in our model are decided quantitatively by the parameters.

If we include the first-order perturbations $\tilde{\phi}_\ell(a)$ in Eq. (D1), and hence corrections to (D4), we can evaluate the anisotropies of the EoS $w_\phi(a)$ of dark energy sourced by the inhomogeneities of ϕ, although these corrections to the isotropic background in Eq. (D4) may be small because of our previous constraints on the amplitudes of ε_1 and ε_2 in Eqs. (85) and (86).

APPENDIX E: LUMINOSITY DISTANCE

Starting from Eq. (87), while still taking the propagation parameter as $\lambda = \chi$, including the normal mode scalar fluctuation $\Psi^{\rm tot} = \Psi^{\rm norm} + \Psi$, to the linear order, we obtain

$$I_{\rm lin}^{\rm tot} = \int_0^{\chi_s} {\rm d}\chi \frac{\chi}{\chi_s}(\chi - \chi_s)\Delta^{(3)}\Psi^{\rm tot}; \tag{E1}$$

but we have Eq. (A10) for Ψ; hence, we only need to consider the cosmological Poisson equation as

$$\Delta^{(3)}\Psi^{\rm tot} = \Delta^{(3)}\Psi^{\rm norm} = 4\pi G\bar{\rho}_m \delta_m a^2. \tag{E2}$$

In gravitationally bound local systems, for example, where objects such as SNe Ia are located, the source term of the scalar perturbations from matter in the Friedmann equation simply reads

$$8\pi G\bar{\rho}_m = 3H^2 = 3H_0^2\Omega_m a^{-3}, \tag{E3}$$

which is identical to Eq. (54); hence,

$$I_{\rm lin}^{\rm tot} = -\frac{3H_0^2\Omega_m}{2}\int_0^{\chi_s} {\rm d}\chi \frac{\chi}{\chi_s}(\chi_s - \chi)a(\chi)^{-1}\delta_m(a(\chi), \boldsymbol{\gamma}). \tag{E4}$$

Because $a^{-1} = 1 + z$ holds by definition between scale factor a and cosmological redshift z, if we only look at the contribution by the inhomogeneous background and

neglect peculiar motion terms, this result is consistent with Eq. (6) in Ref. [57].

APPENDIX F: SOME USEFUL TRANSFORMATION RELATIONS

Here, we provide some useful relations to help transform equations quickly between forms as functions of $\tilde{t}$, a, or η. As we defined the dimensionless quantities in Eqs. (33) and (37),

$$\tilde{t} = H_0 t,$$
$$\tilde{H} = H/H_0,$$

with

$$H = \frac{1}{a}\frac{\mathrm{d}a}{\mathrm{d}t} \tag{F1}$$

as a usual convention. Hence, recalling $'$ is the derivative with respect to a and overdot $\dot{}$ indicates that with respect to η, for arbitrary function $\mathcal{A}$ we have

$$\frac{\partial \mathcal{A}}{\partial \tilde{t}} = \frac{\partial \mathcal{A}}{H_0 \partial t} = a\frac{H}{H_0}\frac{\partial \mathcal{A}}{\partial a} = a\tilde{H}\mathcal{A}', \tag{F2}$$

as well as

$$\frac{\partial \mathcal{A}}{\partial \tilde{t}} = \frac{\partial \mathcal{A}}{H_0 \partial t} = \frac{1}{aH_0}\frac{\partial \mathcal{A}}{\partial \eta} = \frac{\tilde{H}}{aH}\frac{\partial \mathcal{A}}{\partial \eta} = \frac{\tilde{H}}{\mathcal{H}}\dot{\mathcal{A}}. \tag{F3}$$

These will help to transform equations quickly. Following these we have

$$\begin{aligned}\frac{\partial^2 \mathcal{A}}{\partial \tilde{t}^2} &= a\tilde{H}\frac{\partial}{\partial a}\left(a\tilde{H}\frac{\partial \mathcal{A}}{\partial a}\right) \\ &= a^2\tilde{H}^2\mathcal{A}'' + (a^2\tilde{H}\tilde{H}' + a\tilde{H}^2)\mathcal{A}'\end{aligned} \tag{F4}$$

and

$$\frac{1}{a}\frac{\partial a}{\partial \tilde{t}} = \frac{1}{H_0}\frac{1}{a}\frac{\partial a}{\partial t} = H/H_0 = \tilde{H} \tag{F5}$$

as very useful relations.

Finally let us note a universal relation widely used,

$$\dot{\mathcal{A}} = a^2 H\mathcal{A}'. \tag{F6}$$

[1] A. G. Riess *et al.*, Astron. J. **116**, 1009 (1998).
[2] B. P. Schmidt *et al.*, Astrophys. J. **507**, 46 (1998).
[3] S. Perlmutter *et al.*, Astrophys. J. **517**, 565 (1999).
[4] J. R. Gott III, M. S. Vogeley, S. Podariu, and B. Ratra, Astrophys. J. **549**, 1 (2001).
[5] B. Leibundgut, Comput. Phys. Commun. **147**, 459 (2002).
[6] P. J. E. Peebles and B. Ratra, Rev. Mod. Phys. **75**, 559 (2003).
[7] S. Weinberg, Rev. Mod. Phys. **61**, 1 (1989).
[8] D. H. Weinberg, M. J. Mortonson, D. J. Eisenstein, C. Hirata, A. G. Riess, and E. Rozo, Phys. Rep. **530**, 87 (2013).
[9] Y. Akrami *et al.* (Planck Collaboration), Astron. Astrophys. **641**, A1 (2020).
[10] N. Aghanim *et al.* (Planck Collaboration), Astron. Astrophys. **641**, A6 (2020).
[11] S. Tsujikawa, Classical Quant. Grav. **30**, 214003 (2013).
[12] C. Ringeval, T. Suyama, T. Takahashi, M. Yamaguchi, and S. Yokoyama, Phys. Rev. Lett. **105**, 121301 (2010).
[13] D. Glavan, T. Prokopec, and V. Prymidis, Phys. Rev. D **89**, 024024 (2014).
[14] D. Glavan, T. Prokopec, and D. C. van der Woude, Phys. Rev. D **91**, 024014 (2015).
[15] D. Glavan, T. Prokopec, and T. Takahashi, Phys. Rev. D **94**, 084053 (2016).
[16] D. Glavan, T. Prokopec, and A. A. Starobinsky, Eur. Phys. J. C **78**, 371 (2018).
[17] H. Aoki, S. Iso, and Y. Sekino, Phys. Rev. D **89**, 103536 (2014).
[18] H. Aoki and S. Iso, Prog. Theor. Exp. Phys. **2015**, 113E02 (2015).
[19] E. V. Linder, Phys. Rev. D **101**, 023506 (2020).
[20] P. Svrcek and E. Witten, J. High Energy Phys. 06 (2006) 051.
[21] A. Arvanitaki, S. Dimopoulos, S. Dubovsky, N. Kaloper, and J. March-Russell, Phys. Rev. D **81**, 123530 (2010).
[22] G. Obied, H. Ooguri, L. Spodyneiko, and C. Vafa, arXiv: 1806.0836.
[23] P. Agrawal, G. Obied, P. J. Steinhardt, and C. Vafa, Phys. Lett. B **784**, 271 (2018).
[24] S. K. Garg and C. Krishnan, J. High Energy Phys. 11 (2019) 075.
[25] H. Ooguri, E. Palti, G. Shiu, and C. Vafa, Phys. Lett. B **788**, 180 (2019).
[26] S. K. Garg, C. Krishnan, and M. Zaid Zaz, J. High Energy Phys. 03 (2019) 029.
[27] L. Visinelli and S. Vagnozzi, Phys. Rev. D **99**, 063517 (2019).
[28] S. Appleby, R. Battye, and A. Moss, Phys. Rev. D **81**, 081301 (2010).
[29] A. Tripathia, A. Sangwana, and H. K. Jassala, J. Cosmol. Astropart. Phys. 06 (2017) 012.

[30] H. K. Jassal, J. S. Bagla, and T. Padmanabhan, Mon. Not. R. Astron. Soc. **405**, 2639 (2010).
[31] D. Yamauchi, H. Aoki, S. Iso, D.-S. Lee, Y. Sekino, and C.-P. Yeh, J. Cosmol. Astropart. Phys. 05 (2019) 055.
[32] D. J. Schwarz, C. J. Copi, D. Huterer, and G. D. Starkman, Classical Quant. Grav. **33**, 184001 (2016).
[33] P. Fosalba and E. Gaztanaga, Mon. Not. R. Astron. Soc. **504**, 5840 (2021).
[34] L. Polastri, A. Gruppuso, and P. Natoli, J. Cosmol. Astropart. Phys. 04 (2015) 018.
[35] C. Gordon, W. Hu, D. Huterer, and T. Crawford, Phys. Rev. D **72**, 103002 (2005).
[36] R. B. Tully, E. J. Shaya, I. D. Karachentsev, H. M. Courtois, D. D. Kocevski, L. Rizzi, and A. Peel, Astrophys. J. **676**, 184 (2008).
[37] H. M. Courtois, D. Pomarède, R. B. Tully, Y. Hoffman, and D. Courtois, Astron. J. **146**, 69 (2013).
[38] P. da S. Ferreira and M. Quartin, Phys. Rev. Lett. **127**, 101301 (2021).
[39] Y. Akrami *et al.*, Astron. Astrophys. **644**, A100 (2020).
[40] N. J. Secrest, S. von Hausegger, M. Rameez, R. Mohayaee, S. Sarkar, and J. Colin, Astrophys. J. Lett. **908**, L51 (2021).
[41] A. G. Riess, L. MacRi, S. Casertano, H. Lampeitl, H. C. Ferguson, A. V. Filippenko, S. W. Jha, W. Li, and R. Chornock, Astrophys. J. **730**, 119 (2011).
[42] C. L. Bennett *et al.*, Astrophys. J. Suppl. Ser. **208**, 20 (2013).
[43] E. Mörtsell and S. Dhawan, J. Cosmol. Astropart. Phys. 09 (2018) 025.
[44] K. Migkas, G. Schellenberger, T. H. Reiprich, F. Pacaud, M. E. Ramos-Ceja, and L. Lovisari, Astron. Astrophys. **636**, A15 (2020).
[45] K. Migkas, F. Pacaud, G. Schellenberger, J. Erler, N. T. Nguyen-Dang, T. H. Reiprich, M. E. Ramos-Ceja, and L. Lovisari, Astron. Astrophys. **649**, A151 (2021).
[46] C. Krishnan, R. Mohayaee, E. Ó. Colgáin, M. M. Sheikh-Jabbari, and L. Yin, arXiv:2106.02532 [Phys. Rev. D (to be published)].
[47] O. Luongo, M. Muccino, E. Ó. Colgáin, M. M. Sheikh-Jabbari, and L. Yin, arXiv:2108.13228.
[48] Y. Nan, K. Yamamoto, H. Aoki, S. Iso, and D. Yamauchi, Phys. Rev. D **99**, 103512 (2019).
[49] W. Hu, arXiv:astro-ph/9508126.
[50] M. Chevallier and D. Polarski, Int. J. Mod. Phys. D **10**, 213 (2001).
[51] E. V. Linder, Phys. Rev. Lett. **90**, 091301 (2003).
[52] M. Sasaki, Mon. Not. R. Astron. Soc. **228**, 653 (1987).
[53] T. Futamase and M. Sasaki, Phys. Rev. D **40**, 2502 (1989).
[54] H. Aoki, S. Iso, D-S. Lee, Y. Sekino, and C-P. Yeh, Phys. Rev. D **97**, 043517 (2018).
[55] D. Yamauchi, A. Linde, A. Naruko, M. Sasaki, and T. Tanaka, Phys. Rev. D **84**, 043513 (2011).
[56] P. Bielewicz, K. M. Górski, and A. J. Banday, Mon. Not. R. Astron. Soc. **355**, 1283 (2004).
[57] A. Agrawal, T. Okumura, and T. Futamase, Phys. Rev. D **100**, 063534 (2019).
[58] E. Di Valentino, A. Melchiorri, O. Mena, and S. Vagnozzi, Phys. Rev. D **101**, 063502 (2020).
[59] J. T. Nielsen, A. Guffanti, and S. Sarkar, Sci. Rep. **6**, 35596 (2016).
[60] R. Mohayaee, M. Rameez, and S. Sarkar, arXiv:2003.10420.
[61] J. Colin, R. Mohayaee, M. Rameez, and S. Sarkar, Astron. Astrophys. **631**, L13 (2019).
[62] R.-G. Cai, Z.-K. Guo, L. Li, S.-J. Wang, and W.-W. Yu, Phys. Rev. D **103**, L121302 (2021).
[63] D. Rubin and B. Hayden, Astrophys. J. **833**, L30 (2016).
[64] D. Rubin and J. Heitlauf, Astrophys. J. **894**, 68 (2020).
[65] D. E. Holz and S. A. Hughes, Astrophys. J. **629**, 15 (2005).
[66] N. Dalal, D. E. Holz, S. A. Hughes, and B. Jain, Phys. Rev. D **74**, 063006 (2006).
[67] S. Vitale and H. Y. Chen, Phys. Rev. Lett. **121**, 021303 (2018).
[68] X.-N. Zhang, L.-F. Wang, J.-F. Zhang, and X. Zhang, Phys. Rev. D **99**, 063510 (2019).
[69] M. P. Rajvanshi, A. Singh, H. K. Jassal, and J. S. Bagla, Classical Quant. Grav. **38**, 195001 (2021).
[70] M. P. Rajvanshi and J. S. Bagla, Classical Quant. Grav. **37**, 235008 (2020).
[71] P. A. Abell *et al.* (LSST Science Collaborations), arXiv:0912.0201.
[72] R. Laureijs *et al.* (EUCLID Collaboration), arXiv:1110.3193.
[73] D. Spergel *et al.* (WFIRST Collaboration), arXiv:1305.5422.
[74] D. J. Bacon *et al.* (SKA Collaboration), Pub. Astron. Soc. Aust. **37**, E007 (2020).
[75] L. Heisenberg, M. Bartelmann, R. Brandenberger, and A. Refregier, Phys. Rev. D **98**, 123502 (2018).
[76] S. Mizuno, S. Mukohyama, S. Pi, and Y.-L. Zhang, J. Cosmol. Astropart. Phys. 09 (2019) 072.